

OPTIMIZATION OF THREE-DIMENSIONAL ELECTROSPUN
POLYMERS FIBROUS SCAFFOLDS WITH CARBON-BASED
NANOMATERIALS ADDITIVES



A Thesis Submitted in Partial Fulfillment of the Requirements for the
Degree of Master of Science in Applied Physics
Suranaree University of Technology
Academic Year 2022

การหาเงื่อนไขที่เหมาะสมในการสังเคราะห์เส้นใยพอลิเมอร์โครงสร้างสามมิติ
ด้วยสารเติมแต่งที่เป็นวัสดุนาโนคาร์บอน

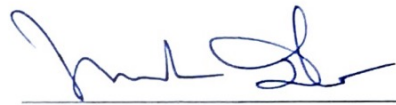


วิทยานิพนธ์นี้เป็นส่วนหนึ่งของการศึกษาตามหลักสูตรปริญญาวิทยาศาสตรมหาบัณฑิต
สาขาวิชาฟิสิกส์ประยุกต์
มหาวิทยาลัยเทคโนโลยีสุรนารี
ปีการศึกษา 2565

OPTIMIZATION OF THREE-DIMENSIONAL ELECTROSPUN POLYMERS
FIBROUS SCAFFOLDS WITH CARBON-BASED
NANOMATERIALS ADDITIVES

Suranaree University of Technology has approved this thesis submitted in partial fulfillment of the requirements for a master's degree.

Thesis Examining Committee



(Assoc. Prof. Dr. Panomsak Meemon)

Chairperson



(Dr. Wiwat Nuansing)

Member (Thesis Advisor)



(Dr. Chatree Saiyasombat)

Member



(Assoc. Prof. Dr. Yupaporn Ruksakulpiwat)

Acting Vice Rector for Academic Affairs

and Quality Assurance



(Prof. Dr. Santi Maensiri)

Dean of Institute of Science

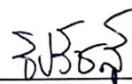
ชิปรัชส์ วิทยกิจพิพัฒน์: การหาเงื่อนไขที่เหมาะสมในการสังเคราะห์เส้นใยพอลิเมอร์โครงร่างสามมิติด้วยสารเติมแต่งที่เป็นวัสดุนาโนคาร์บอน (OPTIMIZATION OF THREE DIMENSIONAL ELECTROSPUN POLYMERS FIBROUS SCAFFOLDS WITH CARBON-BASED NANOMATERIALS ADDITIVES) อาจารย์ที่ปรึกษา : อาจารย์ ดร.วิวัฒน์ นวลสิงห์, 57 หน้า.

คำสำคัญ: อิเล็กโทรสปินนิงแบบสามมิติ, การพิมพ์สามมิติ, เส้นใยพอลิเมอร์, โครงร่างสามมิติ, วัสดุนาโนคาร์บอน

กระบวนการอิเล็กโทรสปินนิงแบบสามมิติ (3D Electrospinning) เป็นเทคนิคที่ใช้ประจุไฟฟ้าเพื่อดึงเส้นใยจากสารละลายพอลิเมอร์และสร้างเส้นใยเป็นโครงร่างในรูปทรงสามมิติ งานวิจัยนี้มีวัตถุประสงค์เพื่อหาเงื่อนไขที่เหมาะสมในการสร้างเส้นใยพอลิเมอร์ให้เป็นโครงร่างแบบสามมิติที่ใกล้เคียงกับรูปร่างต้นแบบหรือรูปร่างที่ออกแบบไว้ ซึ่งกระบวนการอิเล็กโทรสปินนิงแบบสามมิตินี้เป็นกระบวนการที่ดัดแปลงและประยุกต์ใช้เครื่องพิมพ์สามมิติ เพื่อให้สามารถพิมพ์วัสดุให้เป็นโครงร่างเส้นใยสามมิติออกมา โดยใช้เข็มเชื่อมต่อกับอิเล็กโทรดขั้วบวก (พิมพ์ลงบนฐานที่เชื่อมต่อกับอิเล็กโทรดขั้วลบ) ซึ่งได้บรรจุสารละลายพอลิเมอร์ที่ผสมและไม่ผสมสารเติมแต่งวัสดุนาโนคาร์บอนลงในกระบอกฉีดยา โดยสารเติมแต่งเหล่านี้มีสมบัติในการปรับปรุงสมบัติเชิงกลและเชิงชีวภาพของเส้นใยโครงร่างสามมิติ ซึ่งการหาประสิทธิภาพของสารเติมแต่งนี้มีการจำแนกลักษณะและการตรวจสอบสารเติมแต่งที่เป็นวัสดุนาโนคาร์บอนด้วยกล้องจุลทรรศน์อิเล็กตรอนแบบส่องกราด เทคนิควิเคราะห์การเลี้ยวเบนของรังสีเอ็กซ์ และเทคนิคฟูเรียร์ทรานส์ฟอร์มอินฟราเรดสเปกโทรสโกปี นอกจากนี้ยังมีการเปรียบเทียบสมบัติระหว่างเส้นใยพอลิเมอร์โครงร่างสามมิติที่มีสารเติมแต่งวัสดุนาโนคาร์บอนกับไม่มีสารเติมแต่ง โดยใช้เครื่องทดสอบเชิงกลและการทดสอบที่ได้กล่าวมาข้างต้น รวมถึงยังมีการใช้อิเล็กโทรดนำทางในการสร้างเส้นใย เพื่อให้ผลลัพธ์ที่ออกมาใกล้เคียงกับต้นแบบมากขึ้น ซึ่งผลจากการวิจัยในครั้งนี้พบเงื่อนไขที่เหมาะสมในการสร้างเส้นใยคือ อัตราการไหลของสารละลายที่ 10 มิลลิลิตรต่อชั่วโมง., ขนาดเข็ม 18G ระยะทางระหว่างเข็มถึงฐาน 5 เซนติเมตร และแรงดันไฟฟ้าที่ใช้ 10-12 กิโลโวลต์ โดยผลจากงานวิจัยนี้ช่วยให้สามารถพัฒนากระบวนการผลิตและทำความเข้าใจถึงผลกระทบของสารเติมแต่งวัสดุนาโนคาร์บอนต่อผลลัพธ์ที่เป็นเส้นใยพอลิเมอร์โครงร่างสามมิติ

สาขาวิชาฟิสิกส์
ปีการศึกษา 2565

ลายมือชื่อนักศึกษา



ลายมือชื่ออาจารย์ที่ปรึกษา

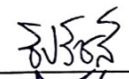
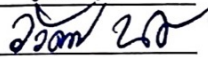


TIPRAT VITAYAKITPIPAT : OPTIMIZATION OF THREE-DIMENSIONAL ELECTROSPUN POLYMERS FIBROUS SCAFFOLDS WITH CARBON-BASED NANOMATERIALS ADDITIVES. THESIS ADVISOR : WIWAT NUANSING, Ph.D. 57 PP.

Keyword: 3D electrospinning, 3D printing, polymer fibers, 3D fibrous scaffold, carbon-based nanomaterials

Three-dimensional (3D) electrospinning is a scientific technique that uses electrical charges to draw a scaffold from a polymer solution and allowing scaffolds to be fabricated in a 3D shape. This research aims to find the most appropriate parameters that can fabricate 3D polymer fibrous scaffolds that closely resemble the original or 3D-designed shape. The 3D electrospinning method employs modified 3D printing to print scaffolds, utilizing a positive electrode-connected needle (printed into the negative electrode-connected base) and a syringe containing a polymer solution with the inclusion of carbon-based nanomaterial additives. These additives offer the potential to enhance the mechanical and biological properties of the 3D scaffolds. To investigate the effectiveness of the additives, five different types of characterization techniques, including scanning electron microscopy (SEM), X-ray diffraction (XRD), and Fourier-transform infrared spectroscopy (FTIR) were used to classify each type of additive. Additionally, a comparison is made with 3D scaffolds fabricated with and without any additives. Furthermore, polymer scaffolds fabricated using 3D electrospinning techniques were characterized and compared using mechanical testing machines and the characterizations mentioned above. In the electrospinning process, a guiding electrode was used to accelerate the 3D build-up process. Through this investigation, the most appropriate parameters that were suitable for this research are 10 mL/h of flow rate, 18 G of needle size, 5 cm of distance from the collector to the needle tip distance, and 10-12 kV of applied voltage. And the fabrication process can be optimized, and carbon-based nanomaterial additives can affect on the resulting 3D polymer scaffolds.

School of Physics
Academic Year 2022

Student's Signature 
Advisor's Signature 

ACKNOWLEDGEMENTS

First of all, I would like to give my sincere thanks to my thesis advisor, Dr. Wiwat Nuansing for his continuous help and constant encouragement throughout this research. He has taught and guided me many things. Especially the methodology to carry out the research as clearly as possible.

In addition, I am so grateful for all members of 3D Electrospinning Tech (3DET) laboratory. They gave me much advice and helps for the 3D electrospinning machine problems and the research.

I would like to specially mention to Development Promotion of Science and Technology (DPST) for the scholarship since I was in high school until now.

I also give a special thanks to Spray' De team and Student Entrepreneurship Development Academy (SEDA) for financial supports and experience about the entrepreneurship.

I also express my sincerely thanks to my colleagues for their supports and advice.

Finally, I am also extremely grateful to my family for their love, time, supports throughout the period of this research.

Tiprat Vitayakitpipat

CONTENTS

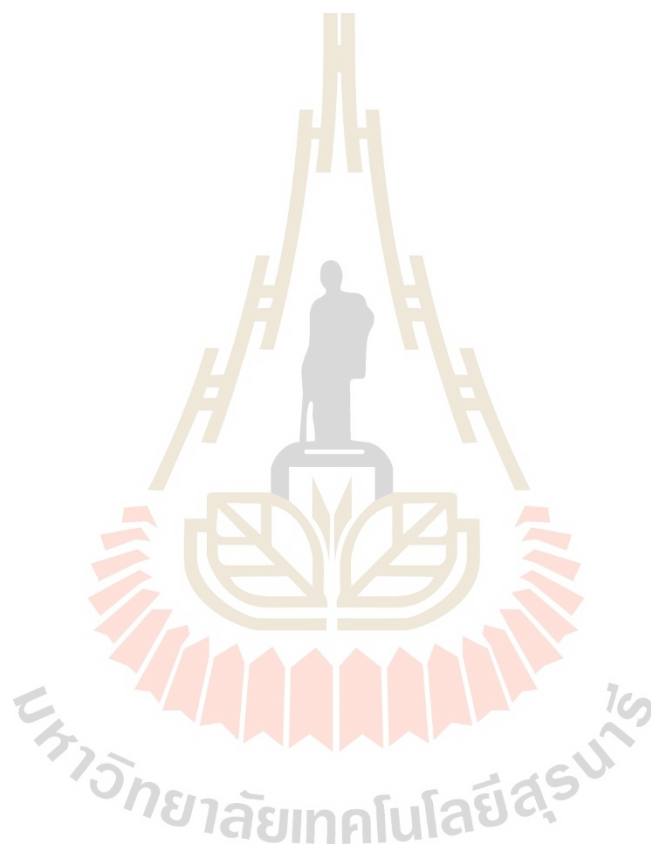
	Page
ABSTRACT IN THAI	I
ABSTRACT IN ENGLISH	II
ACKNOWLEDGEMENTS	III
CONTENTS.....	IV
LIST OF TABLES	VII
LIST OF FIGURES	VIII
LIST OF ABBREVIATIONS	XI
CHAPTER	
I INTRODUCTION	1
1.1 Research objectives	2
1.2 Research hypotheses	2
II LITERATURE REVIEWS	3
2.1 Polymers	3
2.2 Solvents	4
2.3 Carbon-based nanomaterial	6
2.4 3D electrospinning	8
2.5 Parameters of 3D electrospinning	8
2.6 Electrode configurations	10
2.7 Characterizations	13
2.7.1 Mechanical properties	13
2.7.2 Morphology.....	15
2.7.3 Fourier-Transform-Infrared (FTIR) spectroscopy	16
2.7.4 X-Ray diffraction (XRD) spectroscopy	19

CONTENTS (Continued)

		Page
III	MATERIALS AND METHODS.....	21
	3.1 Solution preparations.....	21
	3.2 Fiber fabrication (3D electrospinning technique)	21
	3.3 Characterizations	23
	3.3.1 The tensile test	23
	3.3.2 The morphological test.....	24
	3.3.3 The X-ray diffraction test (XRD)	24
	3.3.4 The Fourier-Transform infrared spectroscopy (FTIR).....	25
IV	RESULTS.....	26
	4.1 Solution preparations results	26
	4.2 Fiber fabrication (3D electrospinning technique) results	27
	4.3 Characterizations results.....	38
	4.3.1 Tensile test.....	38
	4.3.2 Morphology tests.....	39
	4.3.3 XRD results.....	40
	4.3.4 FTIR results	41
V	CONCLUSION.....	43
	REFERENCES.....	46
	APPENDICES.....	49
	APPENDIX A SOLVENTS, POLYMERS, CARBON-BASED NANOMATERIALS AND 3D ELECTROSPINNING EQUIPMENTS THAT USED IN THIS RESEARCH.....	53

CONTENTS (Continued)

	Page
APPENDIX B THE 26 TH INTERNATIONAL ANNUAL SYMPOSIUM ON COMPUTATIONAL SCIENCE AND ENGINEERING (ANSCSE26) CONFERENCE ABSTRACT	56
CURRICULUM VITAE	57



LIST OF TABLES

Table		Page
2.1	The mechanical properties of electrospun PCL membrane using various solvents ratios. All cases, PCL concentration of 15wt%, tip to collector distance of 20cm, flow rate of 0.5mL/h and applied voltage 15kV were maintained	15
4.1	The solutions preparation results.....	26
4.2	The fabrication results of sample PL11 with 10mL/h flow rate.....	27
4.3	The fabrication results of sample PL11 with 5mL/h flow rate.....	28
4.4	The fabrication results of sample PL9 with 18G needle and 10mL/h flow rate	28
4.5	The fabrication results of sample PL9 with 20G needle, 5mL/h flow rate and 10mL/h flow rate.....	29
4.6	The fabrication results of sample PL9 result with 6cm diameter guiding electrode (guiding A), 7cm diameter guiding electrode (guiding B) and 10cm diameter guiding electrode (guiding C).....	30
4.7	The fabrication results of sample PL12 without carbon-based nanomaterial added	31
4.8	The fabrication results of sample PL7 result with same parameters as Figure 4.1(i) with 10mL/h of flow rate.....	33
4.9	The fabrication results of sample PL8 result with same parameters as Figure 4.1(i) with 10mL/h of flow rate.....	33
4.10	The fabrication results of sample PL9 result with same parameters as Figure 4.1(i) with 10mL/h of flow rate.....	34
4.11	The fabrication results of sample PL10 result with same parameters as Figure 4.1(i) with 10mL/h of flow rate.....	35
4.12	The fabrication results of sample PL11 result with same parameters as Figure 4.1(i) with 10mL/h of flow rate.....	36

LIST OF FIGURES

Figure		Page
2.1	Typical Transmission Electron Microscope (TEM) micrograph of electrolytically exfoliated graphene.....	7
2.2	a.) Electrospinning set-up integrated with the flat square collector. b.) Electrospinning set-up integrated with the rotating drum collector. And 1.) Syringe pump, 2.) Needle tip, 3.) The collector, 4.) Zoom in the needle tip to collector distance.....	9
2.3	The electrode configurations that were used the base electrode, a.) 5cm of flat circle around the nozzle, b.) 10cm of flat circle around the nozzle and c.) 5.5cm of the ring around the nozzle. The steering electrode is d.) 5.5cm of the ring floating between the nozzle and the collector by floating in 2.5cm above the collector. And the guiding electrodes, e.) two of 4cm x 5cm rectangles and f.) 5.5cm of the ring is placed on the collector.....	11
2.4	Results of based electrodes in 3D electrospinning. a.) High FPS camera photograph and a.1) electric field simulations of electrospinning with a 5cm aluminum foil circle base electrode, where b.) and b.1) 10cm aluminum foil circle and, c.) and c.1) 5.5cm aluminum ring. The base electrodes decrease the whipping motion of the electrospun jet, resulting in a wet line.....	11
2.5	The result of steering electrode on 3D electrospinning. a.) High FPS camera photograph and b.) The electric field simulation of electrospinning with a 5.5cm aluminum ring electrode. As no voltage is applied to the ring, the electrospun jet can converge to it.....	12
2.6	The guiding electrode results on 3D electrospinning, a.) High FPS camera photograph and a.1) Electric field simulations of electrospinning with two parallel aluminum rectangles. b.) High FPS camera photograph and b.1) Electric field simulations of electrospinning with a 5.5cm aluminum ring put on the collector. The guiding electrodes help to shape the electrospun 3D structure.....	13

LIST OF FIGURES (Continued)

Figure	Page
2.7	Stress-strain behavior of electrospun PCL membrane using various ratio of solvents. All cases, PCL concentration of 15wt%, tip to collector distance of 20cm, flow rate of 0.5mL/h and applied voltage 15kV were maintained.....14
2.8	SEM micrographs for the PCL scaffolds with concentrations of 5, 7.5 and 10%w/v when electrospun with flow-rate of 0.05mL/min.....15
2.9	SEM images of electrospun PCL membranes using acetone as the solvent. 10wt% PCL (a) and 15wt% PCL (b) solutions electrospun at a tip to collector distance of 15cm, an applied voltage of 18kV and a flow rate of 1mL/h. Graphs represent the frequency of diameter distribution16
2.10	FTIR spectra of electrospun polystyrene(PS) fibers, with(3D) and without (flat) HCL additive. No significant shifts in peaks are observed.....17
2.11	FTIR analysis of graphene oxide (GO) nano powders at the different absorbed doses.....18
2.12	FTIR analysis of graphite (black color line)and FTIR analysis of graphene oxide (orange color line).....18
2.13	(a) X-Ray diffraction patterns of graphite powder and GO and (b) X-Ray diffraction patterns of PCL and GO-PCL composite.....19
3.1	(a) The syringe was connected to the long tube and the needle; (b) the syringe pump was pumped the solution out; (c) the wire was connected to the needle tip and the collector and to DC power supply; (d) the cylindrical aluminum foil guiding electrode.....22
3.2	Instron tensile tester model 5565.....23
3.3	Auriga series Carl Zeiss scanning electron microscopy.....24
3.4	Rigaku smartLab x-ray diffractometer (XRD).....24
3.5	Bruker Tensor27 FTIR spectroscope.....25
4.1	(a) Sample PL11 result with 10mL/h flow rate; (b) Sample PL11 result with 5mL/h flow rate; (c) Sample PL9 result with 18G needle and 10mL/h flow rate; (d) Sample PL9 result with 20G needle and 5mL/h flow rate; (e) Sample PL9 result with 20G needle and 10mL/h flow rate;

LIST OF FIGURES (Continued)

Figure	Page
(f) Sample PL9 result with 6cm diameter guiding electrode; (g) Sample PL9 result with 7cm diameter guiding electrode; (h) Sample PL9 result with 10cm diameter guiding electrode; (i) Sample PL12 result without carbon-based nanomaterial added; (j) Sample PL7 result with same parameters as Figure 4.1(i); (k) Sample PL8 result with same parameters as Figure 4.1(i); (l) Sample PL9 result with same parameters as Figure 4.1(i); (m) Sample PL10 result with same parameters as Figure 4.1(i); (n) Sample PL7 result with same parameters as Figure 4.1(i).....	37
4.2 The stress-strain chart between the carbon-based nanomaterials (G1) added scaffold (sample PL7), (G2) added scaffold (sample PL8), (G3) added scaffold (sample PL9), (G4) added scaffold (sample PL10), (G5) added scaffold (sample PL11) and the scaffold that has no carbon-based nanomaterial added (sample PL12).....	39
4.3 The SEM image of 3D electrospinning scaffold.....	39
4.4 (a) G1 carbon- based nanomaterial SEM image; (b) G2 carbon- based nanomaterial SEM image; (c) G3 carbon- based nanomaterial SEM image; (d) G4 carbon- based nanomaterial SEM image; (e) G5 carbon- based nanomaterial SEM image.....	40
4.5 XRD patterns of carbon-based nanomaterials G1-G5 that added in the solutions. (In Figure 4.5, Graphene01 refers to G1 carbon-based nanomaterial, to Graphene05 refers to G5 carbon-based nanomaterial).....	41
4.6 FTIR spectra of carbon-based nanomaterials G1-G5 that added in the solutions. (In Figure 4.6 Graphene01 refers to G1 carbon-based nanomaterial, to Graphene05 refers to G5 carbon-based nanomaterial).....	42
A1 1 liter of 99.9 % Dimethyl sulfoxide.....	50
A2 (a) 2.5 liters of Acetone; (b) 2.5 liters of ethanol; (c) 2.5 liters of methanol	50
A3 (a) 250g of polycaprolactone; (b) 150g of polyvinyl alcohol; (c) 1kg of polylactic acid (powder); (d) bottle of polylactic acid (pill).....	54
A4 5 unknown carbon-based nanomaterials (G1-G5).....	54
A5 (a) 10mL of syringe; (b) 18G and 20G needles.....	55
A6 3D electrospinning machine.....	55

LIST OF ABBREVIATIONS

3D	Three dimensional
SEM	Scanning electron microscope
XRD	X-ray diffraction
FTIR	Fourier transform infrared
PCL	Polycaprolactone
PVA	Polyvinyl alcohol
PLA	Polylactic acid
PGA	Polyglycolide
PHEA-PLA	poly(N-2-hydroxyethyl)-dl-aspartamide–polylactic acid
FDM	Fused deposition modeling
DMSO	Dimethylsulfoxide
DMF	Dimethylformamide
CHCl ₃	Trichloromethane or chloroform
CNTs	carbon nanotubes
THF	Tetrahydrofuran
TEM	Transmission electron microscope
rGO	Reduced graphene oxide
GO	Graphene oxide
PS	Polystyrene
PAN	Polyacrylonitrile
PVP	Polyvinylpyrrolidone
MeOH	Methyl alcohol or methanol
FPS	Frame per second
2D	two dimensional
HCL	Hydrochloric acid
CH ₂	Methylene
CH	Benzene
COOH	carboxylic acids
SP	Shot peening
G0-G5	Unknown carbon-based nanomaterial zero to five

CHAPTER I

INTRODUCTION

Three-dimensional (3D) printing stands as an additive manufacturing method, crafting tangible items from digital blueprints. This technique involves depositing fine tiers of substance, which can be in the shape of fluid or powdery plastic, metal, or cement, and subsequently melding these tiers to form a cohesive whole. The 3D printing has been used in many industries such as science, medicine, and construction etc. The electrospinning technique is a scaffold fabrication method that uses the electrical charge to draw a very fine scaffold from the polymer solutions. It also can be used in many industries as well, such as medicine and science. And the combination of the 3D printing and the electrospinning is called the 3D electrospinning technique. It is a technique that uses the electrical charge to fabricate a scaffold from the polymer solution and can be fabricated the scaffolds in 3D shape. To fabricate the 3D scaffolds that has the similar shape to the original 3D designed shape, the polymer solutions and the most appropriate parameters that affects directly to the scaffold results (such as the needle size, flow rate, applied voltage, needle tip to the collector distance) have to be suitable for the 3D scaffolds results.

This research work will investigate and find the polymer solutions and the most appropriate parameters that are suitable for the 3D scaffold results. In addition, three-dimensional (3D) electrospinning will be used to fabricate 3D scaffolds using polymer solution with carbon-based nanomaterials additions. The carbon-based nanomaterials will be used as an additive because this carbon-based nanomaterial can enhance mechanical properties of the 3D scaffolds. Several research reports presented that scaffold containing appropriated amounts of carbon-based nanomaterials have the higher tensile strength than that do not contained carbon-based nanomaterials. Furthermore, polymer scaffolds fabricated by the 3D electrospinning techniques with and without the carbon-based nanomaterials would be compared by using the mechanical testing machine. And the 5 unknown carbon-based nanomaterials would be characterized by using the SEM, FTIR and XRD as well. This research would show the most appropriate fabricating parameters that are suitable for the 3D scaffolds

fabrication and the unknown carbon-based nanomaterials characterizations.

1.1 Research objectives

1.1.1 To find the new polymer solution with/without the carbon-based nanomaterials addition that can be fabricated the 3D polymer fibrous scaffold.

1.1.2 To fabricate 3D fibrous scaffolds from polymer solution that are similar to the prototype file by using 3D electrospinning technique.

1.1.3 To investigate the physical and chemical properties of the carbon-based nanomaterials additions in the 3D polymer fibrous scaffolds with/without the carbon-based nanomaterials addition for the characterization and identification of each type of the additions in solutions.

1.2 Research hypotheses

1.2.1 The optimization of a new polymer solution, with or without the addition of carbon-based nanomaterials, enables the fabrication of 3D polymer fibrous scaffolds.

1.2.2 The implementation of a novel fabrication process, utilizing 3D electrospinning techniques, allows for the creation of 3D polymer fibrous scaffolds that closely resemble the desired 3D prototype shape.

1.2.3 A comprehensive understanding of the physical and chemical properties of carbon-based nanomaterial additions in 3D polymer fibrous scaffolds, both with and without such additions, facilitates their characterization and identification, enabling differentiation between the various types of additions in solution.

CHAPTER II

LITERATURE REVIEWS

2.1 Polymers

Based on the findings of previous research on polymer electrospinning, it was observed that the initial polymer solutions did not yield satisfactory results, necessitating the development of a new polymer solution. Firstly, finding the new polymer that is biocompatibility like polycaprolactone (PCL), so polyvinyl alcohol (PVA) and polylactic acid (PLA) was found. Then the new suitable solvent had to be found for each polymer. The biocompatibility and biodegradability of polylactic acid (PLA) have been extensively researched. Over the past two decades, biodegradable polymers like PLA, PGA, and polycaprolactone (PCL) have emerged as a class of biomaterials garnering increased attention in surgical applications, drug delivery, and tissue engineering. These applications include sutures for wound healing, internal fixation devices for bone structures, carriers for controlled release of bioactive molecules, and scaffolds for tissue or organ regeneration. The synthetic copolymer PHEA-PLA possesses unique properties that render it suitable for crafting biocompatible scaffolds, without compromising cell viability. Monte, A. I. L., Licciardi, M., Bellavia, M., Damiano, G., Palumbo, V. D., Palumbo, F. S., ... Giammona, G. (2012) Polylactic acid (PLA) stands as a bioabsorbable polymer extensively employed in the production of bioabsorbable implants, such as pins, plates, and screws. These implants gradually degrade within the body primarily through hydrolysis, coinciding with the progression of bone union. PLA also finds application as a fundamental material in Fused Deposition Modeling (FDM) for crafting 3D-printed objects. Nevertheless, certain limitations exist that could curtail the utilization of 3D-printed PLA within the medical domain. Notably, PLA possesses a relatively hydrophilic nature, which can lead to reduced cell affinity and occasional elicitation of inflammatory reactions upon direct interaction with surrounding tissues. Saniei, H. and Mousavi, S. (2020). Polylactic acid (PLA) has low hydrophilicity. Liu, Y., Wang, S., Lan, W., and Qin, W. (2018). From Zhang, W., Huang, C., Kusmartseva, O., Thomas, N. L., and Mele, E. (2017), Polylactic acid (PLA) was solubilized using acetone at a concentration of 15% w/v. This study further

introduced tea tree oil or manuka oil into the PLA/acetone solution at five distinct concentrations: 2.5% v/v, 5.0% v/v, 7.5%v/v, 10.0%v/v and 15.0%v/v for antibacterial activity and mechanical properties improvements. According to Saavedra, J. P., Ricaurte, L., Perez, N. C. P., and Carvajal, M. X. Q. (2022), Polyvinyl alcohol (PVA) represents a synthetic polymer possessing optimal traits for fabricating fibers. It boasts biodegradability, biocompatibility, water solubility, and robust chemical and thermal stability. Notably, polyvinyl alcohol (PVA) is a non-toxic polymer, receiving approval from the Food and Drug Administration (FDA) for applications involving materials in direct contact with food. Polyvinyl alcohol (PVA) does exhibit certain drawbacks, including relatively modest mechanical attributes and limited thermal stability. However, these shortcomings can be effectively mitigated by incorporating graphene, resulting in a notable enhancement of these properties. Ginestra, P., Riva, L., Fiorentino, A., Zappa, D., Comini, E., and Ceretti, E. (2019). In Saavedra, J. P., Ricaurte, L., Perez, N. C. P., and Carvajal, M. X. Q. (2022) research, polyvinyl alcohol (PVA) is dissolved with the distilled water at a temperature of $90^{\circ}\text{C} \pm 5^{\circ}\text{C}$ in the concentration of 8 %w/v, the dispersions were agitated until it is fully dissolved and cooled at 65°C . And from (Saniei, H. and Mousavi, S. (2020)), polyvinyl alcohol (PVA) is dissolved with water into three different concentrations of 5wt%, 8wt% and 10wt% at the temperature of 90°C .

2.2 Solvents

According to the polymers in 2.1, the appropriate solvents that can dissolve each polymer have been found. At first, acetone was used as the solvent of polycaprolactone (PCL). Acetone is a relatively ecofriendly and less-toxic solvent compared to other organic solvents. But there are only few reports regarding the use of acetone in order to fabricate the scaffold. Agarwal, S. and Greiner, A., (2011) therefore, acetone was used as the solvent in this research work and acetone mixed with water had been used, also dimethyl sulfoxide (DMSO) which are seen as alternative non-toxic solvents, DMSO is water soluble and it could be diffused into water very quickly. Jia, W. J., Gu, Y. C., Gou, M. L., Dai, M., Li, X. Y., Kan, B., ... Qian, Z. Y. (2008), it is produced in nature and is known to be a source of carbon and sulfur. It is used in many experiments such as pharmaceutical preparations, biological experiments and of course, as a polymer solvent. and it must be carefully used at high concentration. Kim, K. and Lee, S. E. (2020). And DMSO with acetone combined was used to be the solvent of polycaprolactone. For polyvinyl alcohol (PVA), acetone and acetonitrile were used as the solvent. Acetonitrile is much less toxic due to its stable C-CN bond and has been widely used as a polar aprotic solvent in organic synthesis

and purification. Ebrahimlo, A. R. M., and Soreh, P. G. (2019), ethanol or ethyl alcohol that is the organic solvent. Youn, H. S., Kim, S. J., Kim, G. H., and Um, B. H. (2022). Ethanol can be produced by fermentation of sugars and utilized as partial gasoline replacement. It is gaining increasing attention due to its major environment benefits. Elbakush, A. E. and Guven, D. (2020). It also can be produced by reductive carbonylation of methanol. El-Zeftawy, A. M. (1993). And methanol or methyl alcohol. It is a colorless, mobile and neutral liquid with light alcohol smell. It is useful as a drying fluid and completely miscible with water that is much lighter. Methanol is a good solvent for the organic industries, but it is volatile, highly flammable and very toxic chemical. El-Zeftawy, A. M. (1993). It has to be very careful to use methanol as the solvent of PVA. And for polylactic acid (PLA) solvents, acetone, acetone mixed with Dimethylformamide (DMF) was selected as the solvent for this application. DMF finds widespread usage across various industries, including synthetic leather, polyurethane resin, Orlon, and polyacrylic fibers. Renowned as a universal organic solvent, DMF is favored for its exceptional miscibility with water and a wide range of common organic solvents such as toluene, ethyl acetate, and ketones. Nonetheless, it is crucial to note that excessive exposure to DMF has been linked to adverse health effects, encompassing hepatotoxicity, alcohol intolerance, potential embryotoxicity, and teratogenicity in both human and animal subjects. Presently, the permissible exposure limit for DMF concentration within workplace air stands at 10 ppm in the United States and Taiwan. Chang, H. Y., Shih, T. S., Guo, Y. L., Tsai, C. Y., and Hsu, P. C. (2003). The industry that uses DMF as a material, requires the airborne levels in the workplace should not exceed a 10 ppm. 8 h and skin contact be avoided. Hurtt, M. E., Placke, M. E., Killinger, J. M., Singer, A. W., and Kennedy, Jr. G. L. (1991). and also used chloroform as a solvent of PLA. Chloroform, also known as trichloromethane (CHCl_3), is a transparent and colorless chlorinated solvent that exhibits high volatility. It possesses a distinctive odor and a somewhat sweet taste. Due to its sensitivity to light, chloroform is typically stabilized with approximately 0.75% ethanol to prevent its conversion into phosgene and hydrogen chloride through photochemical processes. While it readily dissolves in a wide range of organic solvents, its solubility in water is relatively limited. Luttrell, W. E. (2005). Chloroform is a highly hazardous solvent with potential risks. It can negatively impact reproductive function and contribute to the development of congenital anomalies. Furthermore, chloroform has the capacity to harm vital organs like the kidneys and liver, as well as impair the nervous system. Its effects extend to the circulatory system, potentially leading to severe consequences. Dehghani, M.,

Shahsavani, S., Mohammadpour, A., Jafarain, A., Arjmand, S., Rasekhi, M. A., ... Conti, G. O. (2021).

2.3 Carbon-based nanomaterial

Ever since the discovery of graphene in 2004, a single atom-thick layer of graphitic structure, it has garnered significant attention across numerous domains owing to its exceptional electrical, chemical, and mechanical characteristics. Notably, graphene holds immense potential, particularly when contrasted with other carbon-based materials like carbon nanotubes (CNTs) and graphite. Karuwan, C., Wisitsorrat, A., Phokhratkul, D., Sriprachuabwong, C., Lomas, T., Nacapricha, D., and Tuantranont, A. (2013). Graphene stands as a two-dimensional nano-carbon material, featuring a honeycomb lattice structure that showcases remarkable physical, chemical, and electronic attributes. Sriprachuabwong, C., Karuwan, C., Wisitsorrat, A., Phokhratkul, D., Lomas, T., Sritongkham, P., and Tuantranont, A. (2012). Graphene, being a carbon-based nanomaterial, plays a pivotal role in bolstering the mechanical attributes of fiber mats. This enhancement leads to structural benefits, as graphene contributes to the formation of a non-woven mesh characterized by a substantial surface area per unit mass and a considerable interconnected porosity fraction. Comprising a solitary layer of aromatic carbons, graphene emerges as an exceedingly auspicious contender for generating functionalized electrospun scaffolds. This is largely attributed to the chemical and physical properties inherent to graphene. Ceretti, E., Ginestra, P. S., Ghazinejad, M., Fiorentino, A., and Madou, M. (2017). And in this paper, the graphene was mixed into the 1:1 mixture of tetrahydrofuran (THF) and dimethylformamide (DMF) – polycaprolactone (PCL) solutions with the concentrations of 0.5wt%, 1wt% and 2.0wt% to be compared to each solution.

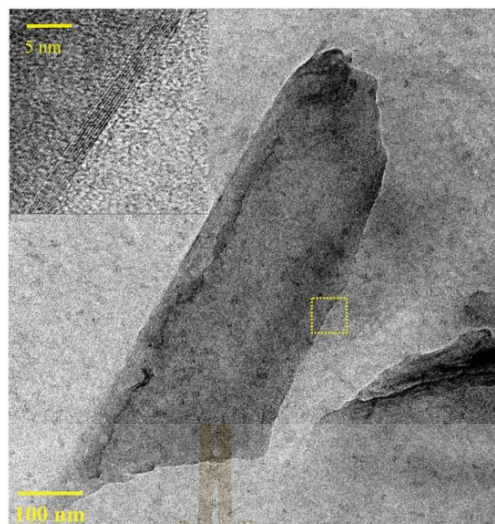


Figure 2.1 Typical Transmission Electron Microscope (TEM) micrograph of electrolytically exfoliated graphene.

According to Figure 2.1, The transmission electron microscopy (TEM) image illustrates the intricate structure of electrolytically exfoliated graphene. The image reveals a thin, polygonal sheet with rounded edges, spanning approximately 250 nm and 800 nm in width and length, respectively. Notably, the sheet exhibits variations in thickness. The identification of this sheet as graphene is corroborated by the high-resolution TEM image. Karuwan, C., Wisitsorrat, A., Phokhratkul, D., Sriprachuabwong, C., Lomas, T., Nacapricha, D., and Tuantranont, A. (2013). And in Ginestra, P., Riva, L., Fiorentino, A., Zappa, D., Comini, E., and Ceretti, E. (2019) research, the study employed reduced graphene oxide (rGO), obtained through the reduction of graphene oxide (GO) via thermal, chemical, or electrical treatments, with rGO generated by eliminating oxygen functional groups from GO. The performance enhancements in graphene-based nanocomposites stem from the imperative of achieving full exfoliation and uniform dispersion of the graphene nanofiller within the matrix. However, it's important to note that graphene's inherent hydrophobic nature restricts its utilization in aqueous-based preparations. Ginestra, P., Riva, L., Fiorentino, A., Zappa, D., Comini, E., and Ceretti, E. (2019). Graphene oxide nanoplatelets (GO) were synthesized from graphite powder using the modified Hummers method. Chaudhuri, B., Mondal, B., Kumar, S., and Sarkar, S. C. (2016).

2.4 3D electrospinning

3D electrospinning is the scaffold fabrication technique that from the combination of 3D printing with electrospinning. 3D printing operates on the principle of layered manufacturing, where materials are progressively deposited layer by layer to create a three-dimensional model. Yan, Q., Dong, H., Su, J., Han, J., Song, B., Wei, Q., and Shi, Y. (2018). It was introduced in the late 1980s to fabricate objects with any complex shape quickly. Chua, C. K., Leong, K. F., and An, J. (2020); Honigsmann, P., Sharma, N., Okolo, B., Popp, U., Msallem, B., and Thieringer, F. M. (2018). Since its inception, the technology has experienced rapid advancement beyond initial expectations, extending its reach beyond mechanical manufacturing into diverse realms of scientific exploration and technological innovation. Notably, 3D printing has demonstrated remarkable utility in the medical domain, including the swift production of customized scaffolds, the creation of organ models, and even direct printing at sites of defects. Kao, C. T., Lin, C. C., Chen, Y. W., Yeh, C. H., Fang, H. Y., and Shie, M. Y. (2015). Nevertheless, practical utilization of 3D printers may encounter certain challenges. For instance, in the medical context, these printers might necessitate specialized materials, a proficient level of technical expertise for operation, and adherence to specific operational parameters, all of which can contribute to elevated production costs.

2.5 Parameters of 3D electrospinning

The key 3D electrospinning parameters considered in this study include flow rate, applied voltage, needle tip to collector distance, needle size, the size and shape of the 3-dimensional file, and printing velocity. To create PVA scaffolds through electrospinning, aqueous PVA solutions with varying concentrations (5wt%, 8wt%, and 10wt%) were formulated at 90°C. The electrospinning process employed a standard 1mL syringe equipped with a 23G stainless steel needle to hold the solutions. Essential electrospinning components encompassed a syringe infusion pump, a power supply, and a grounding electrode. (Saniei, H. and Mousavi, S. (2020)). And in Ginestra, P., Riva, L., Fiorentino, A., Zappa, D., Comini, E., and Ceretti, E. (2019) research,

A solution consisting of 15wt% PVA and 1wt% reduced Graphene Oxide (rGO) was prepared and combined at room temperature. This resulted in a mixture with a PVA:rGO ratio of 3:2, achieved by stirring for 2 hours. The mixture was then loaded into a 10mL syringe affixed with a 21G stainless steel needle. The electrospinning setup is illustrated in Figure 2.2, wherein experiments were conducted using both a square flat collector and a rotating drum collector. The electrospinning process employed a flow

rate of 1mL/h and an applied voltage of 20kV. Scaffolds were collected on the square flat collector, with the distance between the needle tip and collector varying from 20mm to 80mm. Additionally, experiments were conducted on the rotating drum collector to assess potential effects of collector rotation on scaffold diameter and alignment.

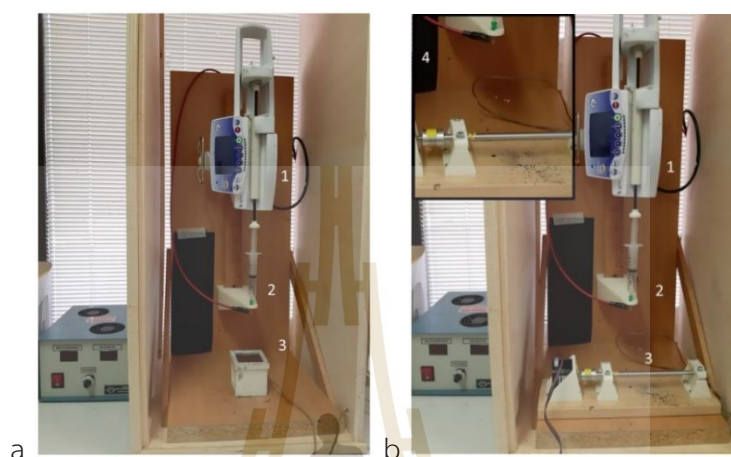


Figure 2.2 a.) Electrospinning set-up integrated with the flat square collector. b.) Electrospinning set-up integrated with the rotating drum collector. And 1.) Syringe pump, 2.) Needle tip, 3.) The collector, 4.) Zoom in the needle tip to collector distance.

For the electrospinning of PCL scaffolds, three uniform solutions containing 15wt% of polycaprolactone (PCL) were prepared by stirring PCL in a blend of tetrahydrofuran (THF) and dimethylformamide (DMF) in a 1:1 ratio. This stirring process was conducted for 24 hours at room temperature. Subsequently, graphene nanoplates at concentrations of 0.5wt%, 1.0wt%, and 2.0wt% were added to the solutions. These mixtures underwent one hour of sonication followed by continued stirring. The resultant solutions were then loaded into a 5mL plastic syringe equipped with a 20G stainless steel needle. The electrospinning process was initiated, applying a flow rate of 0.5mL/h from the syringe and a voltage of 20kV to the needle tip. And the needle tip to the grounded aluminum foil collector distance is 120mm and the experimental procedures were conducted under standard ambient conditions of 25°C temperature and 40% relative humidity. Electrospinning trials were executed, with a duration of 45 minutes for the solution containing 0.5wt% graphene, 30 minutes for the 1.0wt% graphene solution, and merely 15 minutes for the 2.0wt% graphene solution. Beyond these durations, the uniformity of the scaffolds began to deteriorate. Ceretti, E., Ginestra, P. S., Ghazinejad, M., Fiorentino, A., and Madou, M. (2017).

The polymer dissolution process occurred through stirring under ambient conditions. All concentrations were expressed as weight percentages (wt%). Specifically, 15wt% of polystyrene (PS) was dissolved in dimethylformamide (DMF), 15wt% of polyacrylonitrile (PAN) was dissolved in DMF, and 15wt% of polyvinylpyrrolidone (PVP) was dissolved in methanol (MeOH). Each solution maintained a consistent 15wt% concentration. Additives were introduced subsequent to the complete dissolution of the polymer solution, with quantities ranging from 2 μ L to 200 μ L per 20g of solution. Each electrospinning experiment spanned 10 minutes and utilized a fresh polymer solution. Vong, M., Sanchez, F. J. D., Keirouz, A., Nuansing, W., and Radacsi, N. (2021).

2.6 Electrode configurations

In Figure 2.3, to manipulate the electric field, diverse conductive obstructions and supportive materials were directly introduced into the electrospinning chamber. All objects were made with the cardboard and wrapped it in aluminum foil. Regarding shape, several geometries were employed, including flat circles, flat rectangles, and hollow cylinders or rings. These structures were strategically positioned either at the nozzle level or on the collector. Their placement allowed them to function as base, steering, or guiding electrodes, influencing the electrospinning process.

The base electrodes, the 5cm, 10cm of flat circle and 5.5cm of the ring were used. And they were placed around the nozzle for decreasing the size of the deposition area. The steering electrodes, the 5.5cm of the ring was used and floated in the mid-way between the nozzle and the collector for controlling, deflecting the trajectory of electrospinning jet and in Deitzel, J. M., Kleinmeyer, J. D., Hirvonen, J. K., and Beck Tan, N. C. (2001), The implementation of ring electrodes demonstrated a reduction in whipping motion, consequently leading to a more confined deposition area. The guiding electrodes, the 4cm x 5cm rectangles and 5.5cm of the ring were placed directly on the collector for serving as a converging area for electrospinning jet. All electrode configurations are summarized in Figure 2.3.

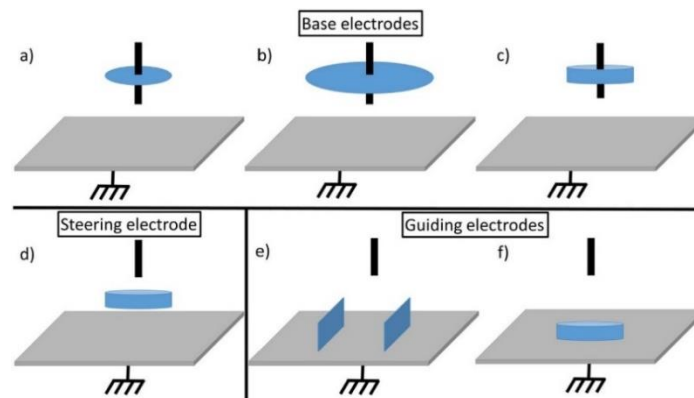


Figure 2.3 The electrode configurations that were used the base electrode, a.) 5cm of flat circle around the nozzle, b.) 10cm of flat circle around the nozzle and c.) 5.5cm of the ring around the nozzle. The steering electrode is d.) 5.5cm of the ring floating between the nozzle and the collector by floating in 2.5cm above the collector. And the guiding electrodes, e.) two of 4cm x 5cm rectangles and f.) 5.5cm of the ring is placed on the collector.

For the results, the electrodes serve the purpose of directing the path of the electrospinning jet, minimizing the deposition area, and altering the electric field's configuration. These factors collectively exert a direct impact on the electrospinning process. In the case of the base electrodes, it was observed that all three shapes were ineffective at achieving uniform fiber electrospinning. Instead, they promoted the development of microbeads and droplets, as depicted in Figure 2.4.

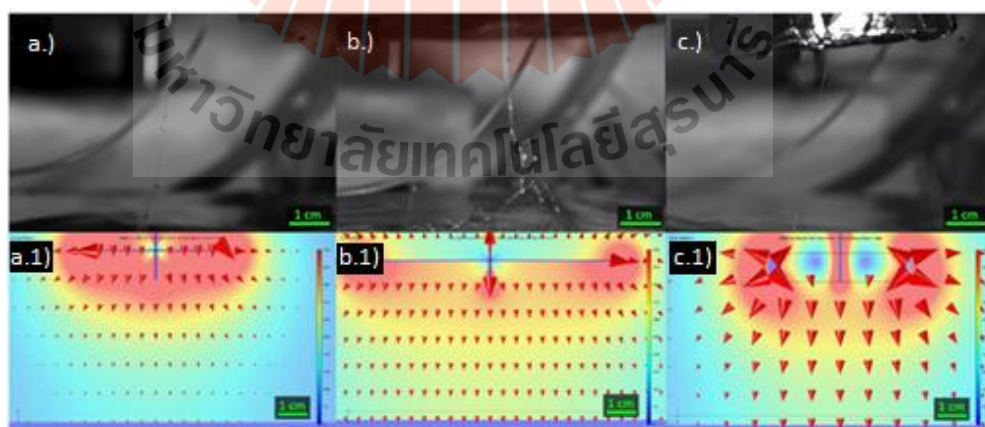


Figure 2.4 Results of based electrodes in 3D electrospinning. a.) High FPS camera photograph and a.1) electric field simulations of electrospinning with a 5cm aluminum foil circle base electrode, where b.) and b.1) 10cm aluminum foil circle and, c.) and c.1) 5.5cm of the ring is placed on the collector.

c.1) 5.5cm aluminum ring. The base electrodes decrease the whipping motion of the electrospun jet, resulting in a wet line.

For the steering electrode results, according to there is no external applied voltage added in the 5.5cm ring of electrode with no connection to the ground, Furthermore, the proximity of the ring electrode to the collector serves as a converging focal point for the electrospun scaffolds just prior to their interaction with the collector surface. This configuration prompts the electrospun jet to converge towards the electrode rather than the collector itself, a phenomenon depicted in Figure 2.5.

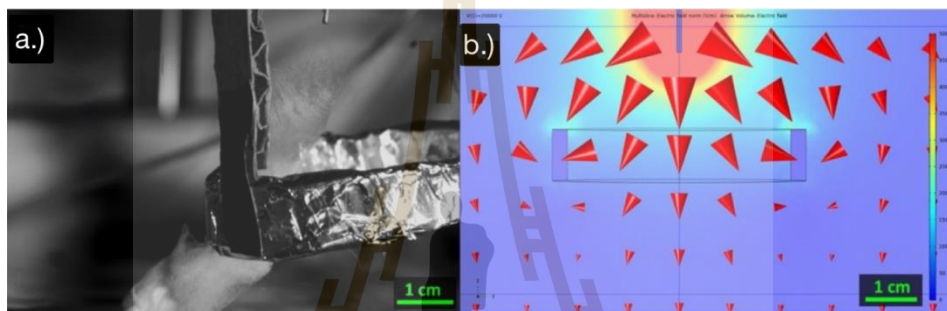


Figure 2.5 The result of steering electrode on 3D electrospinning. a.) High FPS camera photograph and b.) The electric field simulation of electrospinning with a 5.5cm aluminum ring electrode. As no voltage is applied to the ring, the electrospun jet can converge to it.

In the guiding experiments, two rectangular electrodes were utilized to emulate the parallel electrodes of a collector. This arrangement induced scaffold alignment by attracting the electric field lines towards the separated electrodes. Consequently, the scaffolds were directed to converge onto the electrode planes, preventing them from descending to the grounded collector. Meanwhile, the ring electrode positioned within the nozzle's movement region exerted a more pronounced influence on the three-dimensional structure, aligning with the nozzle's trajectory, as depicted in Figure 2.6. This outcome mirrored the characteristics of a cylindrical shape, where no flat scaffold layer converged onto the collector. As a result, this setup expedited the three-dimensional assembly process, yielding enhanced fidelity in shape for the constructed three-dimensional structures. Vong, M., Sanchez, F. J. D., Keirouz, A., Nuansing, W., and Radacsi, N. (2021).

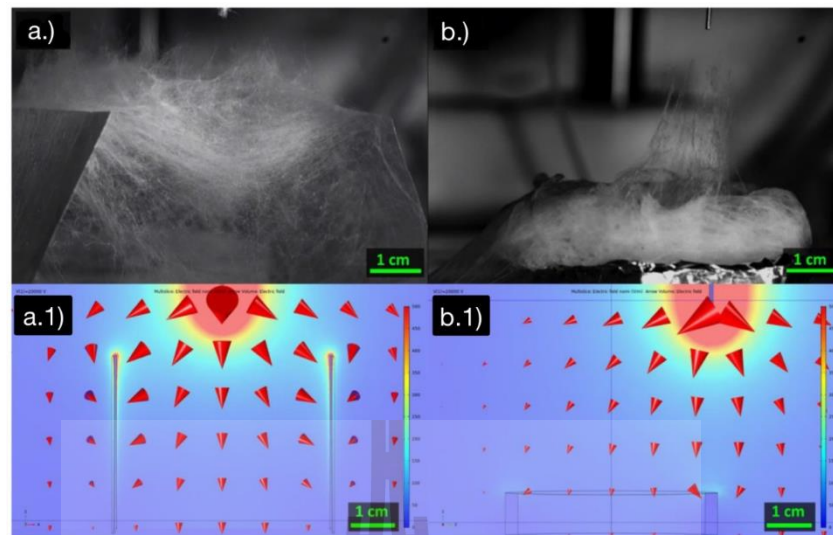


Figure 2.6 The guiding electrode results on 3D electrospinning, a.) High FPS camera photograph and a.1) Electric field simulations of electrospinning with two parallel aluminum rectangles. b.) High FPS camera photograph and b.1) Electric field simulations of electrospinning with a 5.5cm aluminum ring put on the collector. The guiding electrodes help to shape the electrospun 3D structure.

2.7 Characterizations

In this part, the mechanical properties test and the morphological characterization were shown such as SEM and optical characterization such as FTIR and XRD.

2.7.1 Mechanical properties

Firstly, in Cedillo, E. R., Lara, W. O., Pizana, M. R. R., Uribe, J. A. G., Zuniga, A. E., and Rodriguez, C. A. (2019), the analysis of the mechanical strength of the PCL electrospun membranes, according to Halldorson, V. S. N., Steiner, R. L., and Smith, G. B. (2003), rectangular samples were prepared, measuring 5mm in width and 30mm in length, with a width ranging between 0.17mm and 0.35mm. These samples were mounted longitudinally between two gripping units of the tester, providing a 3cm gauge length for mechanical loading. A uniform cross-head speed of 10mm/min was applied to all tested specimens. Mechanical assessment was conducted using an Instron 3365 universal test machine equipped with a 5kN load cell. And for Augustine, R., Kalarikkal, N., and Thomas, S. (2015), The PCL samples were cut into rectangular shapes, each measuring 6x1cm². These samples were mounted vertically between two mechanical gripping units of the tester, allowing for a 3cm gauge length to facilitate mechanical loading. A 500N load cell was applied, and the tests were conducted at a

crosshead speed of 1mm/min. The thickness of each sample was measured using a precision electronic micrometer with an accuracy of $1\mu\text{m}$. Tensile property averages were derived from the outcomes of five tests. The stress-strain curve, illustrated in Figure 2.7, provides a comprehensive insight into the material's tensile properties. Among all the samples tested, the scaffold employing acetone as the sole solvent exhibited the highest break stress, but the lowest modulus. On the other hand, the sample electrospun using acetic acid alone displayed the lowest elongation at break due to the prevalence of beads, resulting in reduced mechanical stability. The PCL scaffold crafted using a 3:7 ratio of acetone and acetic acid achieved the highest elongation prior to breakage and acetic acid also showed the highest toughness as shown in table 2.1.

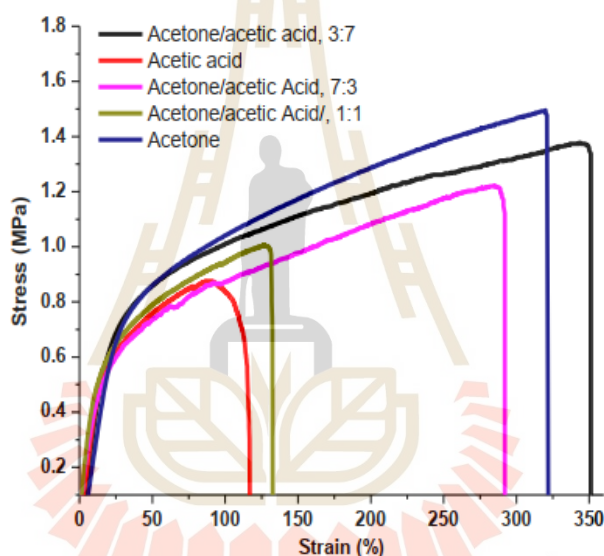


Figure 2.7 Stress-strain behavior of electrospun PCL membrane using various ratio of solvents. All cases, PCL concentration of 15wt%, tip to collector distance of 20cm, flow rate of 0.5mL/h and applied voltage 15kV were maintained.

Table 2.1 The mechanical properties of electrospun PCL membrane using various solvents ratios. All cases, PCL concentration of 15wt%, tip to collector distance of 20cm, flow rate of 0.5mL/h and applied voltage 15kV were maintained.

Solvent	Break stress (MPa)	Elongation at break (%)	Tensile modulus (MPa)	Relative toughness
Acetone	1.45 ± 0.23	323 ± 16	2.1 ± 0.28	362 ± 11
Acetic acid	0.82 ± 0.14	110 ± 13	3.4 ± 0.25	86 ± 6
Acetone and acetic acid in 1:1 ratio	0.99 ± 0.16	130 ± 15	4.7 ± 0.23	104 ± 13
Acetone and acetic acid in 7:3 ratio	1.21 ± 0.26	292 ± 21	3.8 ± 0.27	272 ± 16
Acetone and acetic acid in 3:7 ratio	1.36 ± 0.12	351 ± 17	3.0 ± 0.18	382 ± 8

2.7.2 Morphology

According to Bosworth, L. A. and Downes, S. (2012). in Figure 2.8 and Agarwal, S. and Greiner, A. (2011) in Figure 2.9, the SEM was used for morphological characterization. And to compare the different of the diameter or morphological of the fibers and the SEM will be used in my research as well.

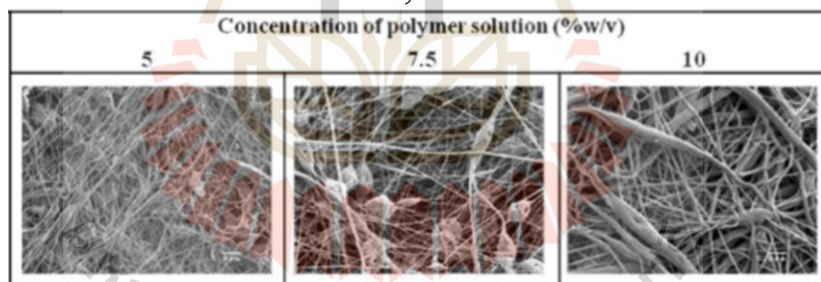


Figure 2.8 SEM micrographs for the PCL scaffolds with concentrations of 5, 7.5 and 10%w/v when electrospun with flow-rate of 0.05mL/min.

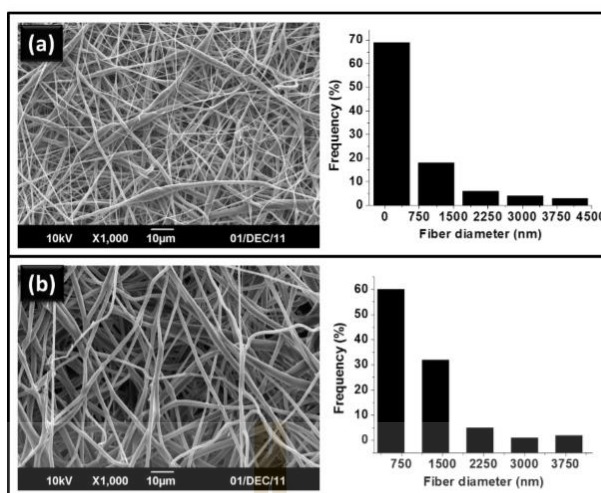


Figure 2.9 SEM images of electrospun PCL membranes using acetone as the solvent. 10wt% PCL (a) and 15wt% PCL (b) solutions electrospun at a tip to collector distance of 15cm, an applied voltage of 18kV and a flow rate of 1mL/h. Graphs represent the frequency of diameter distribution.

2.7.3 Fourier-Transform-Infrared (FTIR) spectroscopy

Fourier-Transform-Infrared (FTIR) spectroscopy is a vibrational spectroscopic method employed to gather insights into the chemical composition of a sample, essentially serving as its "molecular fingerprint." In this study, FTIR was employed to analyze and elucidate the chemical interactions occurring between the polymer, solvent, and additive components. Saavedra, J. P., Ricarte, L., Perez, N. C. P., and Carvajal, M. X. Q. (2022). FTIR spectroscopy has demonstrated its utility in the analysis of various biochemical compounds, particularly for studying changes in the composition of intracellular and extracellular metabolites. This technique allows for the examination of functional groups within cell constituents such as proteins, lipids, carbohydrates, and nucleic acids without necessitating cell disruption. Elbakush, A. E. and Guven, D. (2020). Also, FTIR serves as a potent tool for characterizing chemical alterations, with a distinct ability to identify functional groups within irradiated substances. This technique holds uniqueness in its capability to discern and analyze such changes effectively. Hosseini, M. A., Malekie, S., and Ebranimi, N. (2020).

For example, For the purpose of comparing chemical interactions between the additive and polymer, the FTIR spectra of both two-dimensional (2D) and three-dimensional (3D) polystyrene (PS) fibers were analyzed. The objective was to assess whether significant distinctions emerged as a result of introducing the additive responsible for facilitating the three-dimensional structural formation.

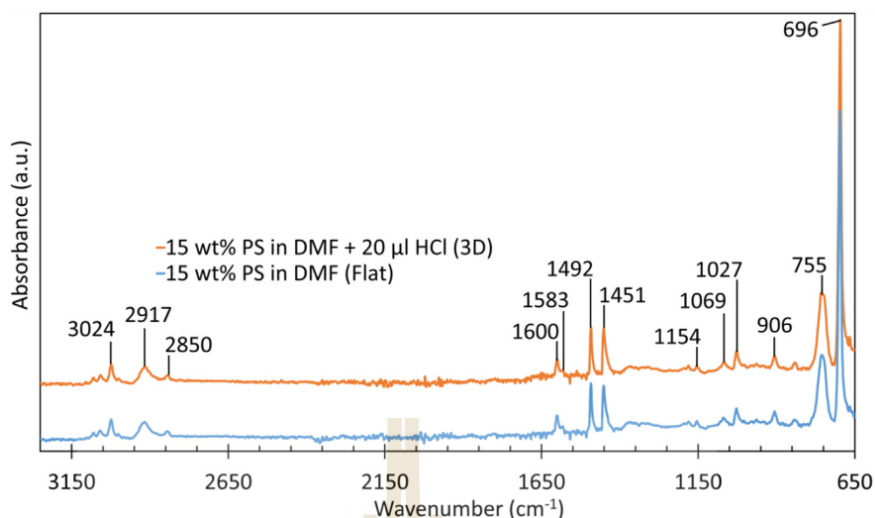


Figure 2.10 FTIR spectra of electrospun polystyrene (PS) fibers, with (3D) and without (flat) HCL additive. No significant shifts in peaks are observed.

As depicted in Figure 2.10, the faint absorption peaks around 3024cm^{-1} arise from the C-H stretching within the benzene ring of PS. The C-H stretching related to the CH_2 and CH groups within the primary PS chain are evidenced by subtle absorption bands at approximately 2917 and 2850cm^{-1} , respectively. Vibrations of the benzene ring manifest at frequencies of 1600 and 1583cm^{-1} , alongside robust peaks observed at 1492 and 1451cm^{-1} . A minor peak at 1154cm^{-1} corresponds to C-H bending in the para-position. Further, the moderate peaks detected at 1069 and 1027cm^{-1} correspond to hydrogen-bending modes within the benzene ring. Lastly, the less pronounced peak at 906cm^{-1} and the robust peaks at 755 and 696cm^{-1} correspond to out-of-plane C-H bending. Regarding the primary PS chain, the stretching mode and bending mode of CH_2 are intertwined with the bands at 2917 and 1451cm^{-1} , respectively. Similarly, C-C stretching interacts with the 1069cm^{-1} band. Vong, M., Sanchez, F. J. D., Keirouz, A., Nuansing, W., and Radacsi, N. (2021). and there are no significant shifts in peak are observed.

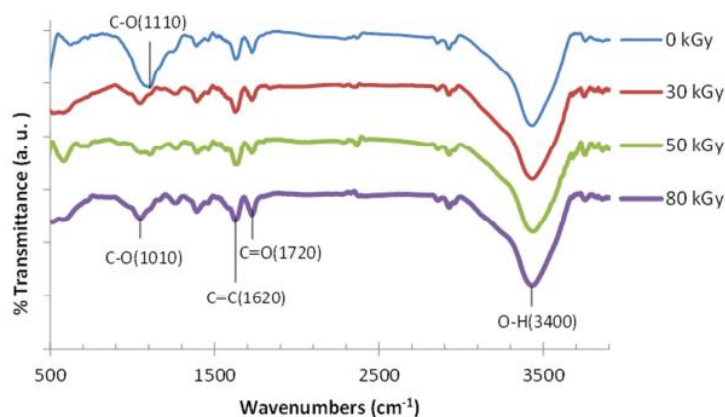


Figure 2.11 FTIR analysis of graphene oxide (GO) nano powders at the different absorbed doses.

In Figure 2.11, the gamma irradiation of nano-graphene oxide powder is depicted within a range of 0–80kGy. The absorption spectra reveal distinct characteristic peaks, including the intense and broad absorption bands at 3400cm^{-1} , attributed to O-H stretching, and in the range of $3500\text{-}3300\text{cm}^{-1}$. Two prominent absorption bands at 1720cm^{-1} and 1620cm^{-1} are particularly noteworthy, corresponding to the skeletal stretching modes of C=O and C=C bonds, respectively. Additionally, peaks at 1010cm^{-1} and 1110cm^{-1} are discernible within the spectra's fingerprint region, likely indicating COOH and C-OH vibration modes, respectively. Hosseini, M. A., Malekie, S., and Ebranimi, N. (2020).

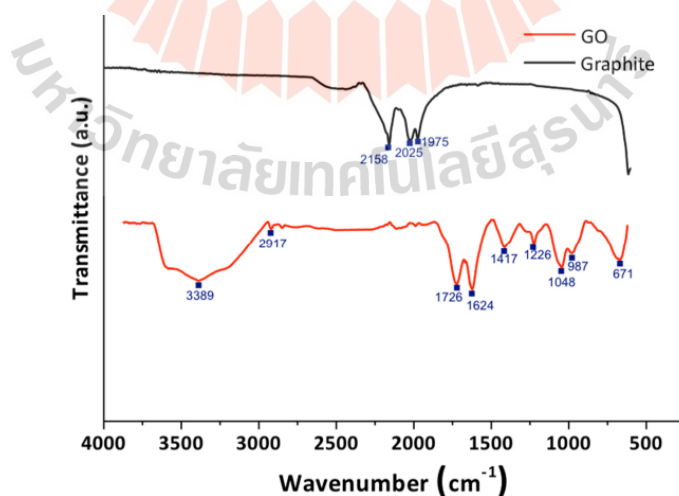


Figure 2.12 FTIR analysis of graphite (black color line) and FTIR analysis of graphene oxide (orange color line).

As seen in Figure 2.12, the FTIR analysis of graphite shows few absorptions signals because the variation in charge distribution among the carbon atoms results in weak differences, giving rise to minor induced dipoles that contribute to a distinct and well-defined spectrum. Notably, the application of oxidation treatment on the material introduces bands corresponding to oxygenated functional groups, affirming the success of the oxidative process. Ruiz, S., Tamayo, J. A., Ospina, J. D., Porras, D. P. N., Zapata, M. E. V., Hernandez, J. H. M., Tovar, C. D. G. (2019).

2.7.4 X-Ray diffraction (XRD) spectroscopy

X-Ray diffraction (XRD) spectroscopy is a non-destructive method used to gather the molecular pattern of a sample. The diffraction angle or direction provides insight into the shape and dimensions of the unit cell, while intensity indicates the arrangement of atoms within the unit cell. Jiang, J., Zhang, S., Longhurst, P., Yang, W., and Zheng, S. (2021). X-Ray diffraction line profile analysis serves as a robust and comprehensive method for characterizing the microstructure of crystalline materials, offering reliability and non-destructiveness to the sample. This approach enables the estimation of domain size within the specimen and quantification of microstrain variations subsequent to Shot Peening (SP) – a surface treatment known for enhancing surface properties of metallic components in industrial settings. This technique proves valuable in assessing the impact of graphene reinforcement on microstructural changes within the composite following SP treatment. Zhan, K., Wu, Y., Li, J., Zhao, B., Yan, Y., Xie, L., Ji, V. (2017). For an example of X-Ray diffraction in Figure 2.13.

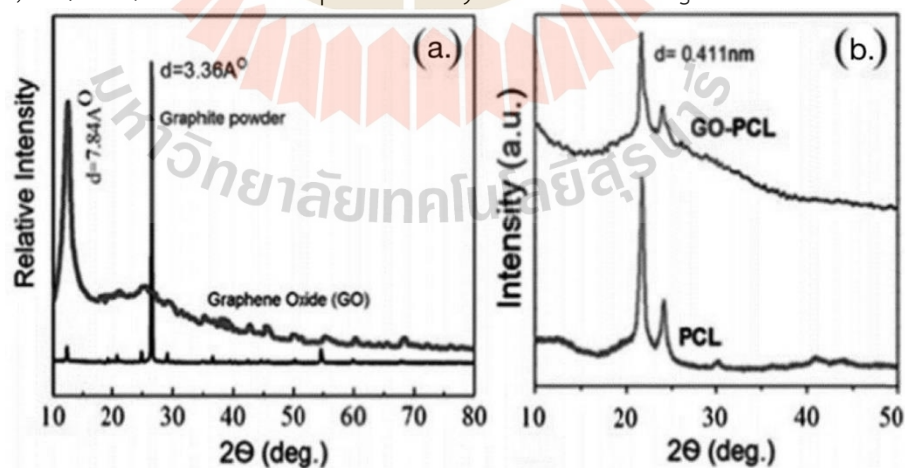


Figure 2.13 (a) X-Ray diffraction patterns of graphite powder and GO and (b) X-Ray diffraction patterns of PCL and GO-PCL composite.

Figure 2.13(a) showcases the X-Ray diffraction patterns of both graphite and Graphene Oxide (GO) for comparative analysis. Notably, the distinctive G peak, positioned at $2\theta = 11.1^\circ$ with a d-spacing of 0.78nm, is absent in the XRD patterns of GO-PCL presented in Figure 2.13 (b.). This absence can be attributed to the disruption of the regular and periodic structure of GO, leading to the development of fully exfoliated structures and a uniform dispersion of GO within the polymer matrix. Chaudhuri, B., Mondal, B., Kumar, S., and Sarkar, S. C. (2016).



CHAPTER III

MATERIALS AND METHODS

3.1 Solution preparations

Polymers that were used in the preparations are Polycaprolactone (PCL), Polyvinyl alcohol (PVA) and Polylactic acid (PLA) (powder and pill appearance). All polymers that were mentioned are the biocompatible polymer which are non-toxic to the human skin and good for the environment. And the solvents that were used to dissolve the polymer are Acetone, Dimethyl Sulfoxide (DMSO), methanol, ethanol, acetonitrile, Dimethylformamide (DMF) and Chloroform. The additives that were added into some solutions are 5 different types of carbon-based nanomaterials. The first step, the additive carbon-based nanomaterials and the solvent were sonicated together in the sonicator bath for 30 minutes by using normal waves for the additive dispersion, then the polymer were added in the solutions and the solutions were stirred at the temperature that suitable for each solvent and each polymer (the temperature is used between 55°C -120°C) until all of the polymer is dissolved in the solvent. But there are some polymers that were not dissolved in the solvent. All solutions that were prepared had 7.3 and 7.5%W/V of concentrations. And the concentration of the carbon-based nanomaterial additions was 0.35%W/V of all solutions.

3.2 Fiber fabrication (3D electrospinning technique)

After the solutions were prepared, the 3D electrospinning technique is used only the completely dissolved polymer solutions to fabricate the fiber. The first step, the 3D prototype file was created by saving it from the Thingiverse.com website and using the Cura program as the slicer program. The printing parameters were set into 0% of the infill, 0°C of nozzle temperature and bed temperature and 0mm of top/bottom thickness to make the hollow cylinder (the easiest shape to be fabricated in 3D electrospinning technique) with the size 5cm of diameter and 5cm of height. After that,

the file was saved in the SD card and put the card in the 3D electrospinning machine. The next step, the z-offset setting was set in the printer to make the distance between the needle tip to the collector. In this study, the parameters were set into 2.5cm and 5cm of the needle tip to the collector distance. Then, a needle was used with the size of (18G, 0.838mm of inner diameter and 20G, 0.603mm of inner diameter.) and 10mL syringe to pump the solution up and the long plastic tube is also connected with the syringe and the needle as in Figure 3.1(a), to make it moves easily when the 3D electrospinning jet is moving.

After that, the syringe was put in the syringe pump to adjust the flow rate (in this research, 3, 5, 7, 8, 9, 10mL/h of flow rate were used) and to pump the solution out. Then, the needle was connected to the 3D electrospinning machine as in Figure 3.1(b), the wire is also connected to the needle tip and the collector to the power supply (positive electrode connected to the needle and negative electrode connected to the collector) as in Figure 3.1(c) to create the electric field for drawing the very fine scaffold from the solution. Then the 3D electrospinning machine were started to print the 3D scaffold, it starts to pump the solution from the syringe pump and the applied voltage was slowly increased from the power supply to fabricate the scaffold and to find the most appropriate parameters (applied voltage, flow rate and needle tip to collector distance) that are suitable to these experiments. And as in Figure 3.1(d), some of the experiments had the guiding electrode to accelerate the 3D build-up process and build 3D structures with higher shape fidelity. Vong, M., Sanchez, F. J. D., Keirouz, A., Nuansing, W., and Radacsi, N. (2021). The guiding electrode is made from the aluminum foil. It had 6cm, 7cm and 10cm diameter with 3cm of height hollow cylindrical shape. The guiding electrode was placed on the middle of the collector when the fabrication started as in Figure 3.1(d).

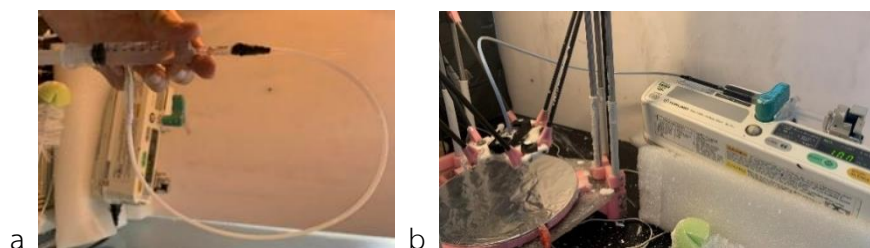


Figure 3.1 (a) The syringe was connected to the long tube and the needle; (b) the syringe pump was pumped the solution out.

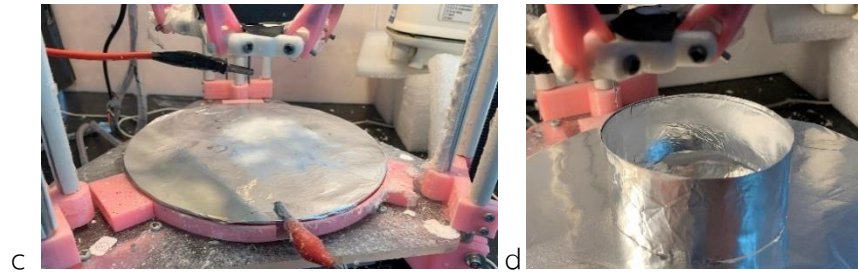


Figure 3.1 (c) the wire was connected to the needle tip and the collector and to DC power supply; (d) the cylindrical aluminum foil guiding electrode (Continued).

3.3 Characterizations

In this research, there are 5 characterizations which are tensile test, morphology test by Scanning Electron Microscope (SEM), X-ray diffraction (XRD), Fourier transform infrared spectroscopy (FTIR).

3.3.1 The tensile test

For the tensile test of the 3D electrospun scaffolds were measured by a universal testing machine as in Figure 3.2



Figure 3.2 Instron tensile tester model 5565.

The first step of the tensile test is cutting all samples into 15x45.00mm of rectangular shape. After that, measured the thickness of each sample and put the magnitude in Merlin program including the velocity of load cells (the 5kN of load cell was used in this research). The load cell velocity was set at 5.00mm/min for all samples. Finally, the sample was fixed in the two grip units of the testing machine and run the machine. After that, the tensile raw data were collected, and the stress-strain graphs were plotted from the raw data in Microsoft Excel.

3.3.2 The morphological test

For the morphological test, the 3D electrospun scaffolds were studied their morphology, such as the scaffold diameter and the surface of the scaffold with a scanning electron microscope (SEM) in Figure 3.3 and the 5 unknown carbon-based nanomaterials were studied the morphology by the scanning electron microscope (SEM) in Figure 3.3 as well.



Figure 3.3 Auriga series Carl Zeiss scanning electron microscopy.

3.3.3 The X-ray diffraction test (XRD)

The XRD spectroscopy was used to characterize the crystallinity of the carbon-based nanomaterials additions in the 3D polymer fibrous scaffolds by putting the sample in the glass holder and put it in the x-ray diffractometer as in Figure 3.4. In this research set the 2θ at 5-90° and 2.4 of the resolutions for all samples. Then OriginPro software was used to create the XRD graph from the raw data.



Figure 3.4 Rigaku smartLab x-ray diffractometer (XRD).

3.3.4 The Fourier-Transform infrared spectroscopy (FTIR)

The FTIR spectroscopy was used to check the chemical properties of the carbon-based nanomaterials additions in the 3D polymer fibrous scaffolds and to classify the 5 unknown carbon-based nanomaterials additions in the FTIR spectroscopy as in Figure 3.5 and the FTIR characterizations were recorded in the wavenumber range of $4000\text{-}400\text{cm}^{-1}$ in transmittance mode at room temperature conditions. Then OriginPro software was used to create the FTIR graph from the raw data.



Figure 3.5 Bruker Tensor27 FTIR spectroscope.



CHAPTER IV RESULTS

4.1 Solution preparations results

From the 3.1 solutions preparation methods above, the results are shown in the table 4.1 below, the solutions that can be fabricated are the sample PC1 and PL6-PL12 due to the polymer solubility.

Some solvents could not dissolve all the polymer and if the polymers were not completely dissolved, it will be caused the needle clogging in the fiber fabrications in the next step.

Table 4.1 The solutions preparation results.

Sample	Polymer	Solvent						Additives	Ratio	Concentration (%w/v)	Stirring temp. (°C)	Solubility	
		acetone	acetonitrile	chloroform	dmf	dmsO	ethanol						methanol
PC1	PCL	✓	-	-	-	✓	-	-	G0*	5:1	7.5	55	✓
PV1	PVA	✓	-	-	-	-	-	-	-	1	7.5	55	X
PV2	PVA	-	✓	-	-	-	-	-	-	1	7.5	55	X
PV3	PVA	-	-	-	-	-	✓	-	-	1	7.5	55	X
PV4	PVA	-	-	-	-	-	-	✓	-	1	7.5	55	X
PL1	PLA (powder)	✓	-	-	-	-	-	-	-	1	7.5	55	X
PL2	PLA (powder)	✓	-	-	✓	-	-	-	-	1:1	7.5	55	X
PL3	PLA (powder)	-	-	✓	-	-	-	-	-	1	7.5	55	X
PL4	PLA (powder)	✓	-	-	✓	-	-	-	-	1:1	7.5	120	X
PL5	PLA (pilI)	✓	-	-	-	-	-	-	-	1	7.5	55	X
PL6	PLA (pilI)	-	-	✓	-	-	-	-	-	1	7.5	55	✓
PL7	PLA (pilI)	✓	-	-	-	-	-	-	G1*	1	7.3	85	✓
PL8	PLA (pilI)	✓	-	-	-	-	-	-	G2*	1	7.3	85	✓
PL9	PLA (pilI)	✓	-	-	-	-	-	-	G3*	1	7.3	85	✓
PL10	PLA (pilI)	✓	-	-	-	-	-	-	G4*	1	7.3	85	✓

Table 4.1 The solutions preparation results (Continued).

PL11	PLA (pil)	✓	-	-	-	-	-	-	G5*	1	7.3	85	✓
PL12	PLA (pil)	✓	-	-	-	-	-	-	-	1	7.5	85	✓

*G0-G5 are the unknown carbon- based nanomaterials.

4.2 Fiber fabrication (3D electrospinning technique) results

After the solutions were well prepared and were fabricated by using the 3D electrospinning technique into the 5 cm of height with 5 cm diameter of the hollow cylindrical shape. These are the results.

Sample PL11; the result that used PLA as the polymer and dissolved by acetone as solvent with 7.3%wt of concentration. This sample was fabricated by 3D electrospinning technique with 18G (0.838 mm of diameter) of needle at 2.5 cm distance between needle tip to collector. The final result as in Figure 4.1(a) shows that it was not performed in the 3D hollow cylindrical shape and had marks caused by sparks. This sample were fabricated with 9mL/h of flow rate and 10kV of applied voltage. And the table 4.2 below has shown the parameter adjustments for these sample.

Table 4.2 The fabrication results of sample PL11 with 10mL/h flow rate.

Flow rate (mL/h)	Applied voltage (kV)	Able to fabricate scaffolds
3	-	X
5	-	X
8	8.0	X
10	8.0	X
10	8.5	X
10	9.0-9.5	Yes, but has little spark

In Figure 4.1(b) is the sample PL11 final result; that used PLA as the polymer and dissolved by acetone as solvent with 7.3%W/V of concentration. It was fabricated with the 18G needle size and the 2.5 cm distance from the collector to needle tip. It was begun to fabricate at 3.44kV of applied voltage with 5mL/h of flow rate. Then the applied voltage was slowly increased and the voltage that gave the best result was 7kV and the flow rate was 5mL/h. The result of these parameters is better than Figure 4.1(a) result. And the result had a ring shape scaffold, but not quite in the 3D hollow

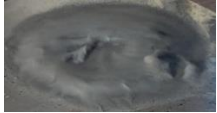
cylindrical shape. And the table 4.3 below has shown the parameter adjustments for these sample.

Table 4.3 The fabrication results of sample PL11 with 5mL/h flow rate.

Flow rate (mL/h)	Applied voltage (kV)	Able to fabricate scaffolds
5	3.44	Better fabrication, when increased the applied voltage
5	6.00	
5	6.50	
5	7.00	

In Figure 4.1(c) is the sample PL9 result that used PLA as the polymer and dissolved by acetone as solvent with 7.3%W/V of concentration. It was fabricated with the 18G needle size and the 5 cm distance from the collector to needle tip. It was begun to fabricate at 10kV of applied voltage with 5mL/h of flow rate. But the flow rate that gave the best result was 10mL/h and the applied voltage was 12kV. The result of these parameters started to fabricate in the 3D hollow cylindrical shape but the height of the scaffold was not stable as in Figure 4.1(c). And the fabrication had an untidy direction when increased the flow rate and applied voltage. And the table 4.4 below has shown the parameter adjustments for these sample.

Table 4.4 The fabrication results of sample PL9 with 18G needle and 10mL/h flow rate.

Flow rate (mL/h)	Applied voltage (kV)	Able to fabricate scaffolds
3	0-15	 Droplet
5	7 10	Start to fabricate scaffolds
7	10-12	Better fabrication, when increased the applied voltage
10	12	
10	13 14	 Untidy direction, when the applied voltage was increased

In Figure 4.1(d) is the sample PL9 result that used PLA as the polymer and dissolved by acetone as solvent with 7.3%W/V of concentration. It was fabricated with the 20G needle size and the 5 cm distance from the collector to needle tip. It was not performed like the 3D hollow cylindrical shape when using 0-20kV of applied voltage and 5mL/h of flow rate. The result had untidy direction of the fabrication and in Figure 4.1(e) is the result of the same sample with the same needle size and distance between needle tip to collector, but the flow rate was 10mL/h. It started to fabricate in the 3D shape with 9kV of the applied voltage and gave the best result at 13kV of the applied voltage with 10mL/h of flow rate. It had an untidy direction fabrication when the applied voltage was higher than 14kV. And the table 4.5 below has shown the parameter adjustments for these sample.

Table 4.5 The fabrication results of sample PL9 with 20G needle, 5mL/h flow rate and 10mL/h flow rate.

Flow rate (mL/h)	Applied voltage (kV)	Able to fabricate scaffolds
5	0-20	 Start to fabricate into 3D shape Better fabrication when increased the applied voltage
	9	
10	10-11	 Best result
	13	
	14	

In Figure 4.1(f) is the sample PL9 result that used PLA as the polymer and dissolved by acetone as solvent with 7.3%W/V of concentration. It was fabricated with the 20G needle size and the 5 cm distance from the collector to needle tip. And this result had the 6cm of diameter hollow cylindrical guiding electrode to accelerate the 3d build-up process. The flow rate that used was 10mL/h and it started to fabricate at 5kV of applied voltage. When the applied voltage was slowly increased to 8kV, it started to fabricate into the outer side of the guiding electrode and when the applied

voltage was increased to 13kV, it started to spark in the outer side of the guiding electrode. And the table 4.6 below has shown the parameter adjustments for these sample.

Table 4.6 The fabrication results of sample PL9 result with 6cm diameter guiding electrode (guiding A), 7 cm diameter guiding electrode (guiding B) and 10 cm diameter guiding electrode (guiding C).

Flow rate (mL/h)	Applied voltage (kV)	Able to fabricate scaffolds
10 + guiding A	5	Start to fabricate a scaffold
	8	Start to fabricate into the outer side of the guiding electrode
	13	Fabricate into the outer side of the guiding electrode and has a little spark later
10 + guiding B	5	Start to fabricate into 3D shape
	7-8	Fiber is fabricated into the edge of the guiding electrode
	10	Start to fabricate into the outer side of the guiding electrode
	12-13	Often fabricate into the outer side of guiding electrode + fabricate the connected fiber into the inner side of guiding electrode
10 + guiding C	5	Droplet
	7	Start to fabricate on the edge of the electrode
	8-9	Start to fabricate into the center of the electrode
	10	Had a little 3D shape on the electrode edge and fabricated scaffolds cover the top of the electrode
	11-13	Start to fabricate into the outer site of the electrode

In Figure 4.1(g) is the sample PL9 result that used PLA as the polymer and dissolved by acetone as solvent with 7.3%W/V of concentration. It was fabricated with the 20G needle size and the 5cm distance from the collector to needle tip. And this result had the 7 cm of diameter hollow cylindrical guiding electrode to accelerate the 3d build-up process. The flow rate that used was 10mL/h and it started to fabricate at 5kV of applied voltage. When the applied voltage was slowly increased to 7- 8kV, it started to fabricate into the edge of the guiding electrode and when the applied voltage was increased to 10kV, it started to fabricate in the outer side of the guiding

electrode. And when the applied voltage was increased to 12-13kV, the scaffold was fabricated the connected scaffold onto the inner side of the guiding electrode as in Figure 4.1(g). And the parameters adjustments of these sample were shown in table 4.6 above.

In Figure 4.1(h) is the sample PL9 result that used PLA as the polymer and dissolved by acetone as solvent with 7.3%W/V of concentration. It was fabricated with the 20G needle size and the 5 cm distance from the collector to needle tip. And this result had the 10 cm of diameter hollow cylindrical guiding electrode to accelerate the 3d build-up process. The flow rate that used was 10mL/h and it started to fabricate droplets at 5kV of applied voltage. When the applied voltage was slowly increased to 7- 8kV, it started to fabricate fine scaffolds onto the edge of the guiding electrode and when the applied voltage was increased to 10kV, it started to fabricate on the inner side of the guiding electrode and had a higher height of the scaffolds. When the applied voltage was increased to 11-13kV, the scaffold was fabricated the connected scaffolds onto the inner side of the guiding electrode as in Figure 4.1(h) with the higher height. And the parameters adjustments of these sample were shown in table 4.6 above.

In Figure 4.1(i) is the sample PL12 that used PLA as the polymer and dissolved by acetone as solvent with 7.5%W/V of concentration without the carbon-based nanomaterials added. It was fabricated with the 18G needle size and the 5 cm distance from the collector to needle tip. With 5mL/h of flow rate, it started to fabricate into the 3D shape at 7kV of applied voltage and when the applied voltage was increased into 8-13kV, the scaffolds had a better fabrication with the fine fibrous scaffolds. With 10mL/h of flow rate, it started to fabricate into the 3D cylindrical shape as in Figure 4.1(i) at 8kV of applied voltage. The scaffold had fine appearance with higher height compared to all results and when the applied voltage increased into 9-10kV, the result had started to fabricate into the bigger cylinder shape with untidy direction. When the applied voltage was increased more than 11kV, the fabrication had more untidy direction. And the table 4.7 below has shown the parameter adjustments for these sample.

Table 4.7 The fabrication results of sample PL12 without carbon-based nanomaterial added.

Flow rate (mL/h)	Applied voltage (kV)	Able to fabricate scaffolds
5	5	Droplet
	7	Start to Fabricate into 3D shape

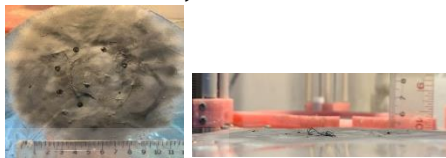
Table 4.7 The fabrication results of sample PL12 without carbon-based nanomaterial added (Continued).

Flow rate (mL/h)	Applied voltage (kV)	Able to fabricate scaffolds
5	8-13	Better fabrication, when increased the applied voltage
	5	Droplet
	8	
10	9-10	Bigger cylinder with untidy direction
	11-15	More untidy direction when increase the applied voltage



In Figure 4.1(j) is the sample PL7 result that used PLA as the polymer and dissolved by acetone as solvent with 7.3%W/V of concentration with the same 3D electrospinning parameters as Figure 4.1(i) with 10mL/h of flow rate. It was fabricated with the 18G needle size and the 5 cm distance from the collector to needle tip. It was begun to fabricate into the scaffolds at 10kV of applied voltage with 10mL/h of flow rate. The applied voltage that gave the best result was 12kV and the flow rate was 10mL/h. The result of these fabrication was not in the 3D cylindrical shape with less than 1 mm of height (which is shorter than the height of sample PL12 without the additives) and with 10 cm of diameter. And the fabrication had an untidy direction when increased the applied voltage over 12kV (the more applied voltage, the more untidy direction). And the table 4.8 below has shown the parameter adjustments for these sample.

Table 4.8 The fabrication results of sample PL7 result with same parameters as Figure 4.1(i) with 10mL/h of flow rate.

Flow rate (mL/h)	Applied voltage (kV)	Able to fabricate scaffolds
10	5-9	Droplet
	10	Start to fabricate into scaffolds
	11	Steady fabrication
	12	
	13-25	 Untidy direction

In Figure 4.1(k) is the sample PL8 result that used PLA as the polymer and dissolved by acetone as solvent with 7.3%W/V of concentration with the same 3D electrospinning parameters as Figure 4.1(i) with 10mL/h of flow rate. It was fabricated with the 18G needle size and the 5 cm distance from the collector to needle tip. It was begun to fabricate into the scaffolds at 8kV of applied voltage with 10mL/h of flow rate. The applied voltage that gave the best result was 10kV and the flow rate was 10mL/h. The result of these fabrication was not in the 3D cylindrical shape with less than 1mm of height (which is shorter than the height of sample PL12 without the additives) and with 14.5 cm of diameter. And the fabrication had an untidy direction when increased the applied voltage over 11kV (the more applied voltage, the more untidy direction). And the table 4.9 below has shown the parameter adjustments for these sample.

Table 4.9 The fabrication results of sample PL8 result with same parameters as Figure 4.1(i) with 10mL/h of flow rate.

Flow rate (mL/h)	Applied voltage (kV)	Able to fabricate scaffolds
10	5-7	Droplet
	8	Start to fabricate into scaffolds
	9	Steady fabrication, but not in 3D shape
	10	

Table 4.9 The fabrication results of sample PL8 result with same parameters as Figure 4.1(i) with 10mL/h of flow rate (Continued).

Flowrate (mL/h)	Applied voltage (kV)	Able to fabricate scaffolds
10	11-25	 Untidy direction

In Figure 4.1(l) is the sample PL9 result that used PLA as the polymer and dissolved by acetone as solvent with 7.3%W/V of concentration with the same 3D electrospinning parameters as Figure 4.1(i) with 10mL/h of flow rate. It was fabricated with the 18G needle size and the 5 cm distance from the collector to needle tip. It was begun to fabricate at 8kV of applied voltage with 10mL/h of flow rate. The applied voltage that gave the best result was 10kV and the flow rate was 10mL/h. The result of these parameters started to fabricate in the 3D cylindrical shape with around 2-3mm of height (which is shorter than the height of sample PL12 without the additives) and with 8.5 cm of diameter. And the fabrication had an untidy direction when increased the flow rate and applied voltage over 11kV. And the table 4.10 below has shown the parameter adjustments for these sample.

Table 4.10 The fabrication results of sample PL9 result with same parameters as Figure 4.1(i) with 10mL/h of flow rate.

Flow rate (mL/h)	Applied voltage (kV)	Able to fabricate scaffolds
	8	Start to fabricate scaffolds
10	10	
	11-25	 Untidy direction

In Figure 4.1(m) is the sample PL10 result that used PLA as the polymer and dissolved by acetone as solvent with 7.3%W/V of concentration with the same 3D electrospinning parameters as Figure 4.1(i) with 10mL/h of flow rate. It was fabricated with the 18G needle size and the 5cm distance from the collector to needle tip. It was begun to fabricate into the scaffolds at 8kV of applied voltage with 10mL/h of

flow rate. The applied voltage that gave the best result was 10kV and the flow rate was 10mL/h. The result of these fabrication was not in the 3D cylindrical shape with less than 1 mm of height (which is shorter than the height of sample PL12 without the additives) and with 12 cm of diameter. And the fabrication had an untidy direction when increased the applied voltage over 11kV (the more applied voltage, the more untidy direction). And the table 4.11 below has shown the parameter adjustments for these sample.

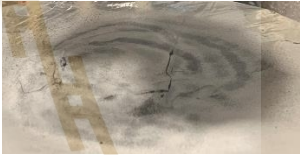
Table 4.11 The fabrication results of sample PL10 result with same parameters as Figure 4.1(i) with 10mL/h of flow rate.

Flow rate (mL/h)	Applied voltage (kV)	Able to fabricate scaffolds
	5-7	Droplet
	8	Start to fabricate into scaffolds
	9	Steady fabrication, but not in 3D shape
10	10	
	11	Not steady in circle fabrication
	12	 Untidy direction
	13-25	More untidy direction, when increased the applied voltage

In Figure 4.1(n) is the sample PL11 result that used PLA as the polymer and dissolved by acetone as solvent with 7.3%W/V of concentration with the same 3D electrospinning parameters as Figure 4.1(i) with 10mL/h of flow rate. It was fabricated with the 18G needle size and the 5 cm distance from the collector to needle tip. It was begun to fabricate into the scaffolds at 8kV of applied voltage with 10mL/h of flow rate. The applied voltage that gave the best result was 10kV and the flow rate was 10mL/h. The result of these fabrication was not in the 3D cylindrical shape with less than 1mm of height (which is shorter than the height of sample PL12 without the additives) and with 12 cm of diameter. And the fabrication had an untidy direction when increased the applied voltage over 11kV (the more applied voltage, the more

untidy direction) and had a little spark when the applied voltage was over than 18kV. And the table 4.12 below has shown the parameter adjustments for these sample.

Table 4.12 The fabrication results of sample PL11 result with same parameters as Figure 4.1(i) with 10mL/h of flow rate.

Flow rate (mL/h)	Applied voltage (kV)	Able to fabricate scaffolds
	5-7	Droplet
	8	Start to fabricate into scaffolds
	9	Steady fabrication, but not in 3D shape
10	10	
	11	Not steady in circle fabrication
	12	
	13-18	More untidy direction, when increased the applied voltage and had a little spark at over 18kV applied voltage

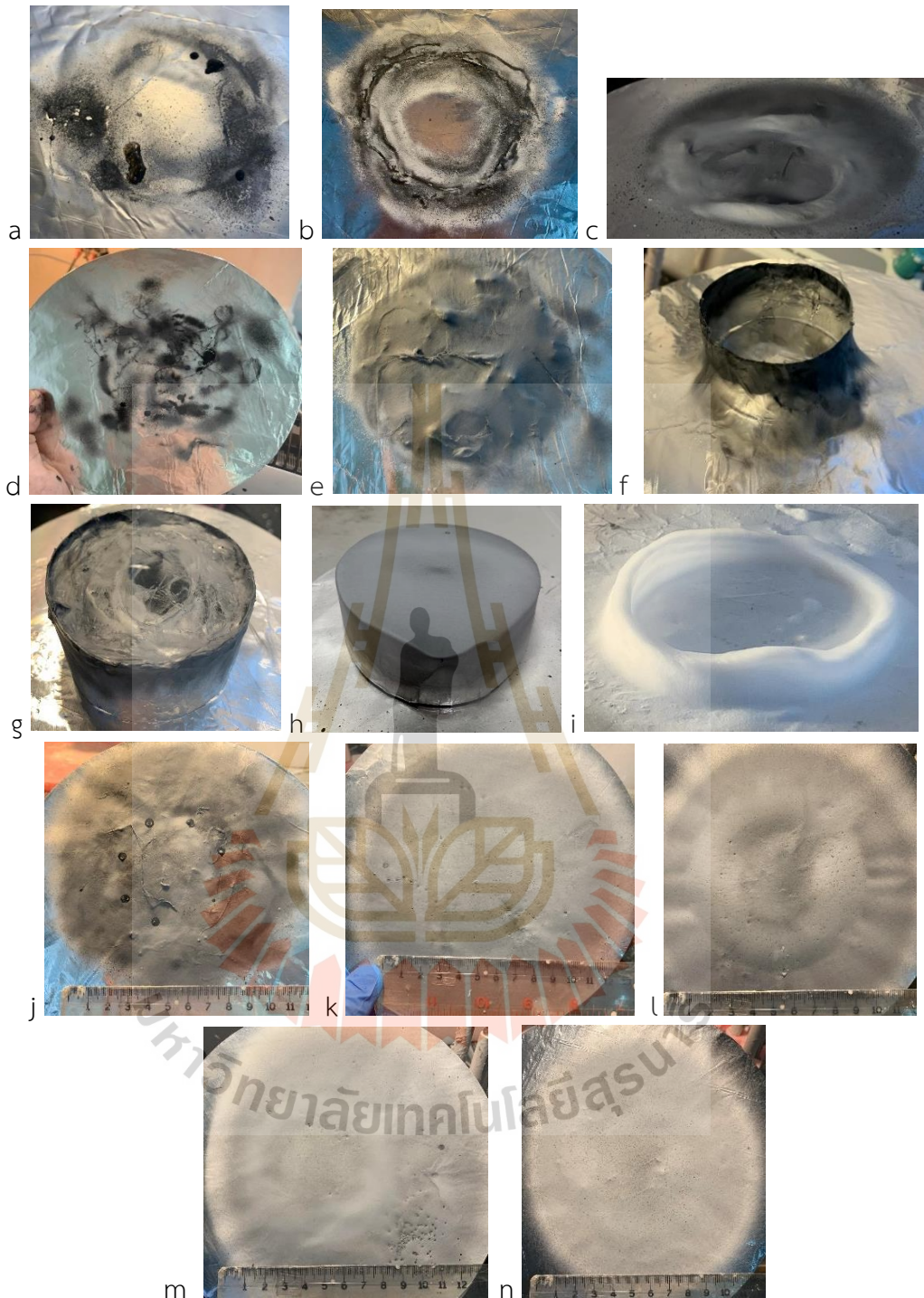


Figure 4.1 (a) Sample PL11 result with 10mL/h flow rate; (b) Sample PL11 result with 5mL/h flow rate; (c) Sample PL9 result with 18G needle and 10mL/h flow rate; (d) Sample PL9 result with 20G needle and 5mL/h flow rate; (e) Sample PL9 result with 20G needle and 10mL/h flow rate; (f) Sample PL9 result with 6 cm diameter guiding electrode; (g) Sample PL9 result with 7 cm diameter guiding electrode; (h) Sample PL9 result with 10 cm diameter guiding electrode; (i) Sample PL12 result without carbon-

based nanomaterial added; (j) Sample PL7 result with same parameters as Figure 4.1(i); (k) Sample PL8 result with same parameters as Figure 4.1(i); (l) Sample PL9 result with same parameters as Figure 4.1(i); (m) Sample PL10 result with same parameters as Figure 4.1(i); (n) Sample PL7 result with same parameters as Figure 4.1(i).

4.3 Characterizations results

4.3.1 Tensile test

The tensile results of the scaffolds were analyzed by the stress-strain chart. The scaffold that has the carbon-based nanomaterials addition compared to the scaffold that has no carbon-based nanomaterial addition as in Figure 4.2. The carbon-based nanomaterial (G1) added scaffold (sample PL7) with the average thickness of 0.256 mm has 63.8564N of the maximum load, 16.63MPa of the maximum stress and 6.63% of the elongation at break. The carbon-based nanomaterial (G2) added scaffold (sample PL8) with the average thickness of 0.225 mm has 52.4711N of the maximum load, 15.55MPa of the maximum stress and 17.17% of the elongation at break. The carbon-based nanomaterial (G3) added scaffold (sample PL9) with the average thickness of 1.731 mm has 60.8197N of the maximum load, 2.34MPa of the maximum stress and 56.88% of the elongation at break. The carbon-based nanomaterial (G4) added scaffold (sample PL10) with the average thickness of 0.290 mm has 59.8151N of the maximum load, 13.75MPa of the maximum stress and 26.68% of the elongation at break. The carbon-based nanomaterial (G5) added scaffold (sample PL11) with the average thickness of 0.184 mm has 56.8944N of the maximum load, 20.61MPa of the maximum stress and 25.14% of the elongation at break. And the scaffold that has no carbon-based nanomaterial addition chart with the average thickness of 2.494 mm has 59.9455N of the maximum load, 1.60MPa of the maximum stress and 57.16% of the elongation at break.

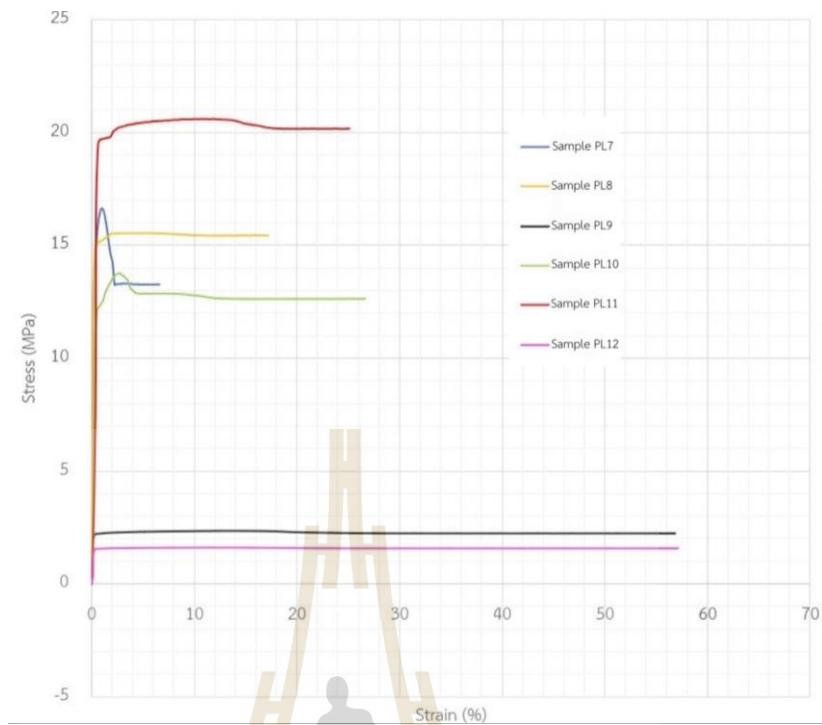


Figure 4.2 The stress-strain chart between the carbon-based nanomaterials (G1) added scaffold (sample PL7), (G2) added scaffold (sample PL8), (G3) added scaffold (sample PL9), (G4) added scaffold (sample PL10), (G5) added scaffold (sample PL11) and the scaffold that has no carbon-based nanomaterial added (sample PL12).

4.3.2 Morphology tests

The morphology of the 3D electrospinning scaffold from sample PL12 without the carbon-based nanomaterials added was analyzed by the scanning electron microscope (SEM) as in Figure 4.3 with 500times of magnification. It shows a very fine fiber overlapping together with the different sizes of fibers around 1-5 μm of width.

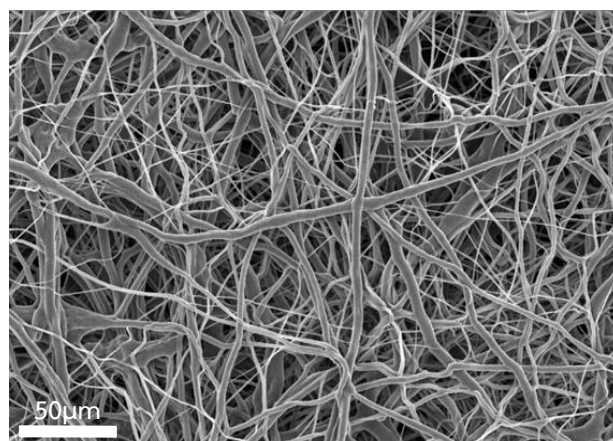


Figure 4.3 The SEM image of 3D electrospinning scaffold.

The morphology of 5 unknown carbon-based nanomaterials were analyzed by SEM as in Figure 4.4 with 10K times magnification. The G1, G2 and G3 carbon-based nanomaterials in Figure 4.4(a), (b), (c) respectively have a tiny flat flake structures which have around 1 μ m of length and the carbon-based nanomaterials agglomerate together. For the G4 and G5 carbon-based nanomaterials in Figure 4.4(d), (e) respectively have the structures like the plane sheets overlapping together and the length size of the G4 and G5 carbon-based nanomaterials are over than 2 μ m.

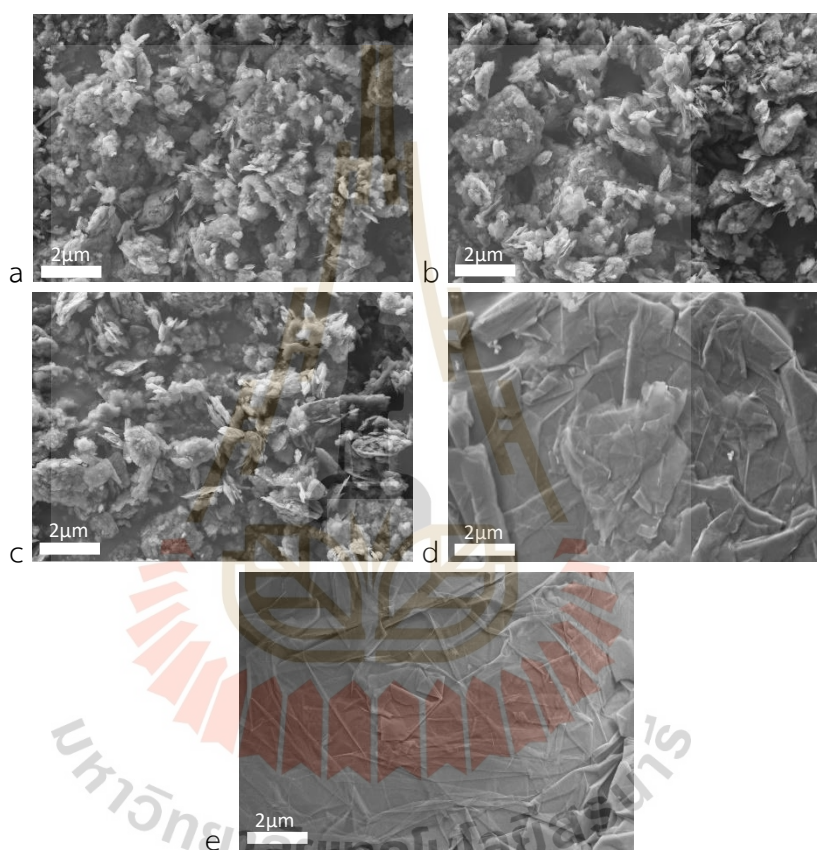


Figure 4.4 (a) G1 carbon- based nanomaterial SEM image; (b) G2 carbon- based nanomaterial SEM image; (c) G3 carbon- based nanomaterial SEM image; (d) G4 carbon- based nanomaterial SEM image; (e) G5 carbon- based nanomaterial SEM image.

4.3.3 XRD results

In this study, the XRD pattern of 5 unknown carbon-based nanomaterials have been analyzed the crystallinity. In Figure 4.5 Shows a shape and tight peak ($2\theta = 26.45^\circ$ and 54.48°) which corresponds to the diffraction line C (002) with the intercellular spacing in the crystal (d) respectively is 3.36 and 3.72 \AA . The XRD patterns

show the data of the typical crystal structure of graphite. Siburian, R., Sihotang, H., Lumban Raja, S., Supeno, M., and Simanjuntak, C. (2017). And there are no significant differences between the 5 carbon-based nanomaterials additives. And the weak peaks in Graphene01-Graphene03, which are indicative of low crystallinity level. Compared to the strong peaks in Graphene04 and Graphene05 that indicated the high crystallinity level. Vong, M., Sanchez, F. J. D., Keirouz, A., Nuansing, W., and Radacsi, N. (2021).

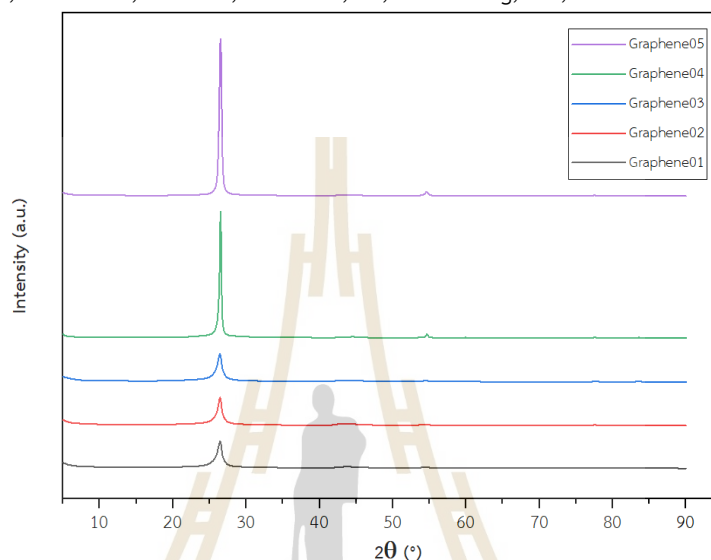


Figure 4.5 XRD patterns of carbon-based nanomaterials G1-G5 that added in the solutions. (In Figure 4.5, Graphene01 refers to G1 carbon-based nanomaterial, to Graphene05 refers to G5 carbon-based nanomaterial).

4.3.4 FTIR results

In this study, the FTIR spectra of 5 unknown carbon-based nanomaterials have been analyzed the chemical interactions in the additives. In Figure 4.6, all spectra show the few absorptions signals due to the difference in the state of charges between carbon atoms. Ruiz, S., Tamayo, J. A., Ospina, J. D., Porras, D. P. N., Zapata, M. E. V., Hernandez, J. H. M., ... Tovar, C. D. G. (2019). The slight variation results in a minor induced electric dipole, contributing to a remarkably clear spectrum. Lopez mata, C., Aguilar, J., and Peña, Y. (2012). The appearance of bands corresponding to oxygenated functional groups following the application of an oxidation treatment unequivocally signifies the successful execution of the oxidative process. Ruiz, S., Tamayo, J. A., Ospina, J. D., Porras, D. P. N., Zapata, M. E. V., Hernandez, J. H. M., ... Tovar, C. D. G. (2019). And from the comparison between the FTIR spectra patterns to Figure 2.12, all FTIR patterns show the data of graphite and there are no significant differences between the 5 carbon-based nanomaterials additives.

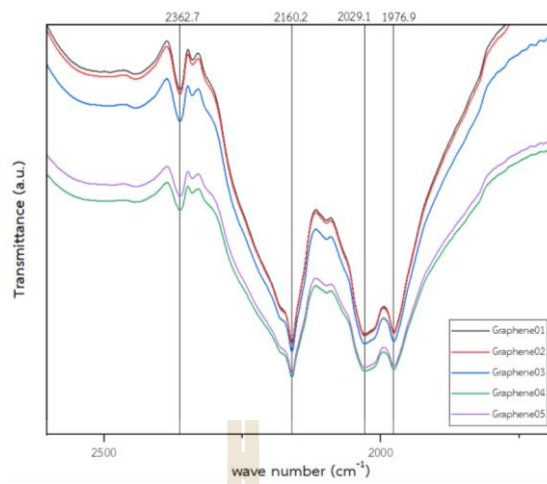


Figure 4.6 FTIR spectra of carbon-based nanomaterials G1-G5 that added in the solutions. (In Figure 4.6 Graphene01 refers to G1 carbon-based nanomaterial, to Graphene05 refers to G5 carbon-based nanomaterial).



CHAPTER V

CONCLUSION

In this study, the solution preparation results in table 4.1. The solutions that can be used to fabricate are sample PC1 that is 7.5%W/V of PCL dissolved with acetone and 0.35%W/V of G0 additive, PL6 that is 7.5%W/V of PLA (pill appearance) dissolved with chloroform without the additive, PL7-PL11 that is 7.3%W/V of PLA (pill appearance) dissolved with acetone and 0.35%W/V of G1-G5 additive (respectively). And sample PL12 that is 7.5%W/V of PLA (pill appearance) dissolved with acetone without the additive. And all the solutions that have PVA and PLA (powder appearance) as polymer cannot be fabricated because the polymer did not be dissolved in the solutions.

The 3D electrospinning scaffolds results as in Figure 4.1(a) and (b) that are the sample PL11 results which has G5 carbon-based nanomaterial added. The shapes of the results are flat and not in 3D hollow cylindrical shape because the distance between the collector is nearby the needle tip and from the G1-G5 carbon-based nanomaterials morphology results in Figure 4.4, G5 carbon-based nanomaterials in Figure 4.4(e) has a big flat sheet flakes that were overlapping together.

In Figure 4.1(d), (e) that are the results from PL9 that has G3 carbon-based nanomaterials added. Figure 4.1(e) that used 10mL/h flow rate has a better scaffold fabrication than Figure 4.1(d) that used 5mL/h flow rate with the same 5 cm of the distance between collector to the needle tip and the same 20G of needle size.

In Figure 4.1(c) that used 18G needle size has a better scaffold fabrication than Figure 4.1(e) that used 20G needle size with the same 5 cm of the distance between collector to the needle tip and 10mL/h of flow rate.

In Figure 4.1(f) and (g), that used the same PL9 sample, the same 20G needle size and the same 5cm of the distance between collector to the needle tip and had a different diameter of the guiding electrode that were 6 cm and 7 cm. The results of these samples are not in the 3D cylindrical shape. The 6 cm diameter guiding electrode result had the scaffolds fabricated in the outer side of the guiding electrode as in Figure 4.1(f) and the 7 cm diameter guiding electrode result had the scaffolds fabricated on the inner side of the guiding electrode as in Figure 4.1(g). And in Figure 4.1(h), that had 10 cm of diameter of the guiding electrode.

The scaffolds were still fabricated only on the top of the guiding electrode due to the electric field in Figure 4.7(b) simulation that the charge will be only on the top of the guiding electrode.

In Figure 4.1(i) and Figure 4.1(j to n), that used the PL12 sample without the additives and used the sample PL7, PL8, PL9, PL10, PL11 respectively, with the same 3D electrospinning parameters (the needle size, the needle tip to the collector distance, the applied voltage and flow rate). The scaffold from the solution that did not have the addition could form into the fine appearance scaffolds with the higher height and in 3D cylindrical shape compared to result in Figure 4.1(j to n). Because the carbon-based nanomaterials additives weighted so that the results that has the carbon-based nanomaterial added could not fabricated into the higher height of the 3D cylindrical shape compared to the result that did not have the additives in Figure 4.1(i) and because the carbon-based nano materials (G1-G5) were made to the low electrical conductivity in the solutions.

In Figure 4.1(j to n), that contained the carbon-based nano materials (G1-G5) respectively. For the results comparisons in Figure 4.1. The shape that had the most-like 3D cylindrical shape is sample PL9 that contained G3 carbon-based nanomaterials with the higher height compared to the sample PL10, PL11, PL7 and PL8 respectively.

From the scaffolds results above, the most appropriate parameters that suitable for this research are 10mL/h of flow rate, 18G of needle size, 5 cm of the distance from the needle to the collector and 10-12kV of applied voltage. And the size of the guiding electrode, the smaller size electrode would have the scaffolds fabricated on the outer size of the electrode and the bigger size electrode would have the scaffolds fabricated on the inner size of the electrode.

The flow rate will vary with the applied voltage for scaffold fabrication. The lower flow rate varies with lower applied voltage, the scaffold results will be stick together and have a shorter height. The higher flow rate varies with the higher applied voltage, the scaffold results will have the higher height but the scaffolds will be loosely overlapping together. But the higher applied voltage can cause the sparks, so the distance between the needle to the collector could be considered to the appropriate distance.

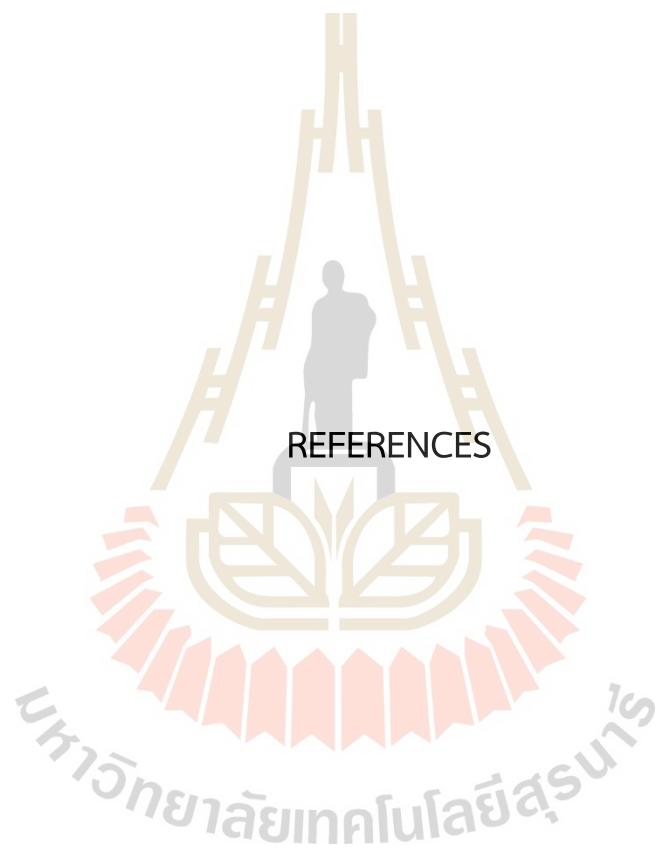
The tensile characterization results, the carbon-based nanomaterial added scaffold has the higher maximum stress and higher maximum load, even the scaffolds thickness is thinner than the no-additives scaffold. The scaffolds that had the highest maximum stress to the lowest are sample PL11(contained G5 additives) > sample PL7(contained G1 additives) > sample PL8(contained G2 additives) > sample

PL10(contained G4 additives) > sample PL9(contained G3 additives) > sample PL12(non-additives). The sample PL7, PL8, PL10, PL11 had lower strains than sample PL9 and sample PL12 due to the scaffolds are brittle. The results could be concluded that the carbon-based nanomaterial additives scaffold has the higher tensile strength than the scaffold that did not have the carbon-based nanomaterial additives. And the carbon-based nanomaterials additives can enhance the mechanical properties (tensile stress) for the scaffold additives.

The morphology results from SEM, shows that the scaffolds that were fabricated from the 3D electrospinning technique had a very fine fiber overlapping together with the different sizes of fibers as in Figure 4.3 And the morphology results of the G1-G5 carbon-based nanomaterial with the same magnification in Figure 4.4, the size of G1, G2 and G3 carbon-based nanomaterial has smaller than G4 and G5 size. The XRD patterns shows that the 5 unknown G1-G5 carbon-based nanomaterial are graphite due to the 2θ peaks that are 26.45° and 54.48° of the results in Figure 4.5 that show the data of the typical crystal structure of graphite. And the weaker peaks in Graphene01-Graphene03, which indicated to the low crystallinity level. Compared to the stronger peaks in Graphene04 and Graphene05 that indicated the high crystallinity level.

The FTIR spectra of 5 unknown carbon-based nanomaterials in Figure 4.6 shows the sparse absorption signals arise from the disparity in the charges between carbon atoms. This subtle distinction results in a minute induced electric dipole, yielding an exceptionally clear spectrum. And all the spectra indicated that 5 unknown carbon-based nanomaterial are graphite and there are no significant differences between the 5 carbon-based nanomaterials additives.

For the suggestions and future works, finding the new 3D electrospinning parameters that can be fabricated the higher height for the carbon-based nanomaterials added solution and using the different type of the electrode to guide the 3D build-up process.



REFERENCES

- Augustine, R., Kalarikkal, N., and Thomas, S. (2015). Clogging free electrospinning of polycaprolactone using acetic acid/acetone mixture. *Polymer-plastics technology and engineering*. doi: 10.1080/03602559.2015.1036451.
- El-Zeftawy, A. M. (1993). Focus on the chemical value of methanol. *J. King Saud Uni*, 7, 209-256.
- Ebrahimlo, A. R. M., and Soreh, P. G. (2019). Rapid and sustainable process with low toxicity for cyanation of silver nitrate by DC arc-discharge in presence of acetonitrile. *Arabian Journal of Chemistry*, retrieved from <http://www.sciencedirect.com>.
- Kolodziej, A., Birczynska, A. W., Swietek, M., Skalniak, L., and Blazewicz, M. (2020). A 2D-Raman correlation spectroscopy study of the interaction of the polymer nanocomposites with carbon nanotubes and human osteoblast-like cells interface. *Journal of Molecular Structure*, retrieved from <https://doi.org/10.1016/j.molstruc.2020.12813>.
- Elbakush, A. E., and Guven, D. (2020). Evaluation of ethanol tolerance in relation to intracellular storage compound of *Saccharomyces cerevisiae* using FTIR spectroscopy. *Process Biochemistry*, retrieved from <https://doi.org/10.1016/j.procbio.2020.11.028>.
- Chaudhuri, B., Mondal, B., Kumar, S., and Sarkar, S. C. (2016). Myoblast differentiation and protein expression in electrospun graphene oxide (GO)-poly (ϵ -caprolactone, PCL) Composite meshes. *Materials Letters*, 194-197. Retrieved from <http://dx.doi.org/10.1016/j.matlet.2016.06.107>.
- Chua, C. K., Leong, K. F., and An, J. (2020). Introduction to rapid prototyping of biomaterials. *Woodhead Publishing Series in Biomaterials*, 1-15. Retrieved from <https://doi.org/10.1016/B978-0-08-102663-2.00001-0>.
- Sriprachubwong, C., Karuwan, C., Wisitsorrat, A., Phokhratkul, D., Lomas, T., Sritongkham, P., and Tuantranont, A. (2012). Inkjet-printed graphene-PEDOT:PSS modified screen printed carbon electrode for biochemical sensing. *Journal of Materials Chemistry*, 5478-5485. doi: 10.1039/c2m14005e.
- Karuwan, C., Wisitsorrat, A., Phokhratkul, D., Sriprachubwong, C., Lomas, T., Nacapricha, D., and Tuantranont, A. (2013). A disposable screen-printed graphe-

- necarbon paste electrode and its application in electrochemical sensing. *RSC Advances*, 3, 25792-25799. Doi: 10.1039/c3ra44187c.
- Kao, C. T., Lin, C. C., Chen, Y. W., Yeh, C. H., Fang, H. Y., and Shie, M. Y. (2015). Poly(dopamine) coating of 3D printed poly (lactic acid) scaffolds for bone tissue engineering. *Materials Science and Engineering C*, 56, 165-173. Retrieved from <http://dx.doi.org/10.1016/j.msec.2015.06.028>.
- Ceretti, E., Ginestra, P. S., Ghazinejad, M., Fiorentino, A., and Madou, M. (2017). Electro Spinning and characterization of polymer-graphene powder scaffolds. *CIRP Annals – Manufacturing Technology*, Retrieved from <http://dx.doi.org/10.1016/j.cirp.2017.04.122>.
- Cedillo, E. R., Lara, W. O., Pizana, M. R. R., Uribe, J. A. G., Zuniga, A. E., and Rodriguez, C.A. (2019). Electrospun Polycaprolactone Fibrous Membranes Containing AG, TiO₂ and Na₂Ti₆O₁₃ Particles for Potntials Use in Bone Regeneration. *Membranes*). Doi: 10.3390/membranes9010012.
- Kazemiparkouhi, F., Karavalakis, G., Falconi, T. M. A., MacIntosh, D. L., and Clark, N. (2022). Comprehensive US database and model for ethanol blend effects on air toxics, particle number, and black carbon tailpipe emissions. *Atmospheric Environment:X*, 16, Retrieved from <https://doi.org/10.1016/j.aeaoa.2022.10185>.
- Saniei, H., and Mousavi, S. (2020). Surface modification of PLA 3D-printed implants by electrospinning with enhanced bioactivity and cell affinity. *Polymer*. doi: <https://doi.org/10.1016/j.polymer.2020.122467>.
- Alharbi, H. F., Luqman, M., Fouad, H., Kha lil, K. A., and Al harthi, N. H. (2018). Viscoelasticbehavior of core-shell structured nanofibers of PLA and PVA produced by coaxial electrospinning. *Polymer Testing*. doi: 10.1016/j.polymertesting. 2018.02.026.
- Youn, H. S., Kim, S. J., Kim, G. H., and Um, B. H. (2022). Enhancing the characteristics of hydrochar via hydrothermal carbonization of Korean native kenaf: The effect of ethanol solvent concentration as co-solvent and reaction temperature. *Fuel*, Retrieved from <https://doi.org/10.1016/j.fuel.2022.125738>.
- Chang, H. Y., Shih, T. S., Guo, Y. L., Tsai, C. Y., and Hsu, P. C. (2003). Sperm function in workers exposed to N, N-dimethylformamide in the synthetic leather industry. *Fertility And Sterility*, 81, 6. doi: 10.1016/j.fertnstert.2003.10.033.
- Deitzel, J. M., Kleinmeyer, J. D., Hirvonen, J. K., and Beck Tan, N. C. (2001). Controlled deposition of electrospun poly (ethylene oxide) fibers. *Polymer*, 42, Retrieved from <https://elsevier.nl/locate/polymer>. Jiang, J., Zhang, S., Longhurst, P., Yang, W., and Zheng, S. (2021). Molecular structure

- Characterization of bituminous coal in Northern China via XRD, Raman and FTIR spectroscopy. *Spectrochimica Acta Part A: Molecular and Biomolecular Spectroscopy*, 255, Retrieved from <https://doi.org/10.1016/j.saa.2021.119724>.
- Saavedra, J. P., Ricaurte, L., Perez, N. C. P., and Carvajal, M. X. Q. (2022). Development And Development and characterization of *Sechium edule* starch and polyvinyl alcohol nanofibers obtained by electrospinning. *Colloids and Surfaces A: Physicochemical and Engineering Aspects*, 649, Retrieved from <https://doi.org/10.1016/j.colsurfa.2022.129456>.
- Zhan, K., Wu, Y., Li, J., Zhao, B., Yan, Y., Xie, L., Wang, L., Ji, V. (2017). Investigation on surface layer characteristics of shot peened graphene reinforced Al composite by X-ray diffraction method. *Applied Surface Science*, 435, 1257-1264. Retrieved from <https://doi.org/10.1016/j.apsusc.2017.11.242>.
- Kim, K., and Lee, S. E. (2020). Combined toxicity of dimethyl sulfoxide (DMSO) and vanadium towards zebrafish embryos (*Danio rerio*): Unexpected synergistic effect by DMSO. *Chemosphere*, 270, Retrieved from <https://doi.org/10.1016/j.chemosphere.2020.129405>.
- Bosworth, L. A., and Downes, S. (2012). Acetone, a Sustainable Solvent for Electrospinning Poly(ϵ -Caprolactone) Fibres: Effect of Varying Parameters and Solution Concentrations on Fibre Diameter. *Journal of Polymers and the Environment*, 20, 879-886. doi: 10.1007/s10924-012-0436-3.
- Hurt, M. E., Placke, M. E., Killinger, J. M., Singer, A. W., and Kennedy, Jr. G. L. (1991). 13-Week Inhalation Toxicity Study of Dimethylformamide (DMF) in Cynomolgus Monkeys. *Fundamental and applied toxicology*, 18, 596-601.
- Dehghani, M., Shahsavani, S., Mohammadpour, A., Jafarain, A., Arjmand, S., Rasekhi, M. A., Conti, G. O. (2021). Determination of chloroform concentration and human exposure assessment in the swimming pool. *Environmental Research*, 203, Retrieved from <https://doi.org/10.1016/j.envres.2021.111883>.
- Vong, M., Sanchez, F. J. D., Keirouz, A., Nuansing, W., and Radacsi, N. (2021). Ultrafast fabrication of Nanofiber-based 3D Macrostructures by 3D electrospinning. *Materials & Design*, 208, Retrieved from <https://doi.org/10.1016/j.matdes.2021.109916>.
- Hosseini, M. A., Malek, S., and Ebranimi, N. (2020). The analysis of linear dose-responses in gamma-irradiated graphene oxide: Can FTIR analysis be considered a novel approach to examining the linear dose-responses in carbon nanostructures?. *Radiation Physics and Chemistry*, Retrieved from <https://doi.org/10.1016/j.radphyschem.2020.109067>.

- Yang, N., Chen, X., Lin, F., Ding, Y., Zhao, J., and Chen, S. (2013). Toxicity formation and distribution in activated sludge during treatment of N, N-dimethylformamide (DMF) wastewater. *Journal of Hazardous Materials*, 264, 278-285. Retrieved from <http://dx.doi.org/10.1016/j.jhazmat.2013.10.002>.
- Othman, N. A. F., Selambakkannu, S., and Seko, N. (2022). Biodegradable dual-layer Polyhydroxyalkanoate (pha)/Polycaprolactone (pcl) mulch film for agriculture: Preparation and characterization. *Energy Nexus*, 8, Retrieved from <https://doi.org/10.1016/j.nexus.2022.100137>.
- Ginestra, P., Riva, L., Fiorentino, A., Zappa, D., Comini, E., and Ceretti, E. (2019). Electrospinning of Poly(vinyl alcohol)-Graphene oxide aligned fibers. *Procedia CIRP*, 89, 110-115. doi: 10.1016/j.procir.2020.05.126.
- Honigsmann, P., Sharma, N., Okolo, B., Popp, U., Msallem, B., and Thieringer, F. M. (2018). Patient- Specific Surgical Implants Made of 3D Printed PEEK: Material, Technology, and Scope of Surgical Application. *BioMed Research International*, Retrieved from <https://doi.org/10.1155/2018/4520636>.
- Monte, A. I. L., Licciardi, M., Bellavia, M., Damiano, G., Palumbo, V. D., Palumbo, F. S., ... Giammona, G. (2012). Biocompatibility and biodegradability of electrospun PHEA- PLA scaffolds: our preliminary experience in a murine animal model. *Digest Journal of Nanomaterials and Biostructures*, 7, 2, 841-851. Retrieved from <https://www.researchgate.net/publication/244280669>.
- Yan, Q., Dong, H., Su, J., Han, J., Song, B., Wei, Q., and Shi, Y. (2018). A Review of 3D Printing Technology for Medical Applications. *Engineering*, 4. doi: <https://doi.org/10.1016/j.eng.2018.07.021>.
- Halldorson, V. S. N., Steiner, R. L., and Smith, G. B. (2003). Residual toxicity after biodegradation: interactions among benzene, toluene, and chloroform. *Ecotoxicology and Environmental Safety*, 57, 162-167. doi: 10.1016/S0147-6513(03) 00032-0.
- Zhang, W., Huang, C., Kusmartseva, O., Thomas, N. L., and Mele, E. (2017). Electrospinning of polylactic acid fibres containing tea tree and manuka oil. *Reactive and Functional Polymers*. doi: 10.1016/j.reactfunctpolym.2017.06.013.
- Jia, W. J., Gu, Y. C., Gou, M. L., Dai, M., Li, X. Y., Kan, B., Yang, J. L., Song, Q. F., Wei, Y. Q., Qian, Z. Y. (2008). Preparation of Biodegradable Polycaprolactone/ Poly (ethylene glycol)/ Polycaprolactone (PCEC) Nanoparticles. *Drug Delivery*, 15, 409-416. doi: 10.1080/10717540802321 727.
- Luttrell, W. E. (2005). Toxic tips: Chloroform. *Chemical Health & Safety*. doi: 10.1016/j.chs.2005.03.002.

- Liu, Y., Wang, S., Lan, W., and Qin, W. (2018). Fabrication of polylactic acid/carbon nanotubes/chitosan composite fibers by electrospinning for strawberry preservation. *International Journal of Biological Macromolecules*, 121, 1329-1336. doi: 10.1016/j.ijbiomac.2018.09.042.
- Ruiz, S., Tamayo, J. A., Ospina, J. D., Porras, D. P. N., Zapata, M. E. V., Hernandez, J. H. M., Valencia, C. H., Zuluaga, F., Tovar, C. D. G. (2019). Antimicrobial Films Based on Nanocomposites of Chitosan/Poly (vinyl alcohol)/Graphene Oxide for Biomedical Applications. *Biomolecules*, 9, 109. doi: 10.3390/biom9030109.
- Siburian, R., Sihotang, H., Lumban Raja, S., Supeno, M., and Simanjuntak, C. (2017). New Route to Synthesize of Graphene Nano Sheets. *Oriental Journal of Chemistry*. Doi: <http://dx.doi.org/10.13005/ojc/340120>.
- Lopez mata, C., Aguilar, J., and Peña, Y. (2012). Caracterización óptica y morfológica de materiales compuestos de P3OT y nanotubos de carbono funcionalizados. *Química Hoy*. 2, 18–23



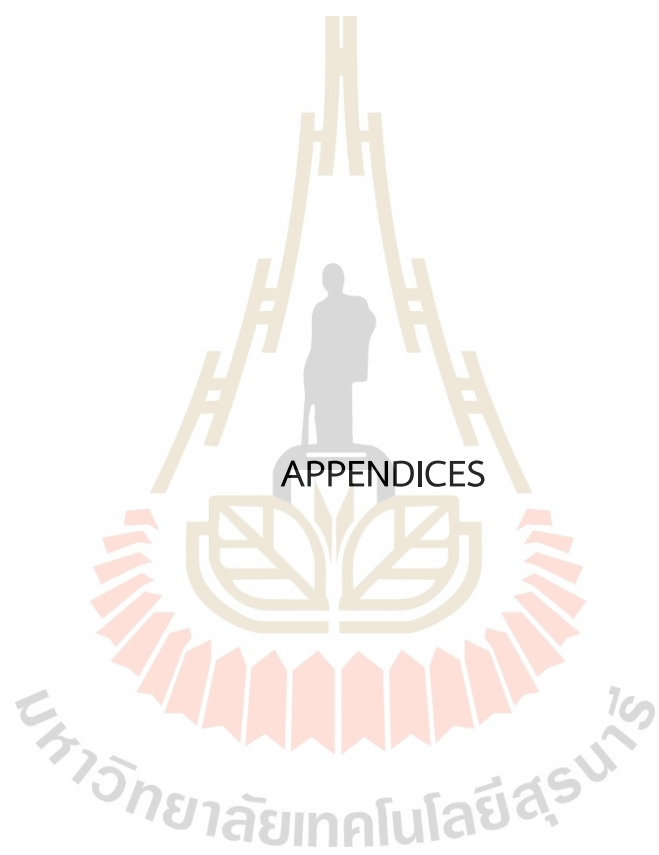




Figure A3 (a) 250g of polycaprolactone; (b) 150g of polyvinyl alcohol; (c) 1kg of polylactic acid (powder); (d) bottle of polylactic acid (pill).



Figure A4 5 unknown carbon-based nanomaterials (G1-G5).



Figure A5 (a) 10mL of syringe; (b) 18G and 20G needles.



Figure A6 3D electrospinning machine.

APPENDIX B

THE 26TH INTERNATIONAL ANNUAL SYMPOSIUM ON
COMPUTATIONAL SCIENCE AND ENGINEERING
(ANSCSE26) CONFERENCE ABSTRACT

The 26th International Annual Symposium on Computational Science and Engineering (ANSCSE26)

20-22 July 2023

**FABRICATION OF THREE-DIMENSIONAL POLYMER FIBROUS SCAFFOLDS
CONTAINING GRAPHENE OXIDE**

Tiprat Vitayakitpipat (lead presenter)¹, Dr. Wiwat Nuansing² *

¹ *School of Chemistry, Institute of Science, Suranaree University of Technology, 111 University Avenue, Muang, Nakhon Ratchasima, 30000, Thailand.*

² *School of Chemistry, Institute of Science, Suranaree University of Technology, 111 University Avenue, Muang, Nakhon Ratchasima, 30000, Thailand.*

*Corresponding address (E-mail: menggtiprat@gmail.com, +66-885942839)

The three-dimensional (3D) electrospinning is a technique that uses the electrical charge to draw a scaffold from the polymer solution and can be fabricated the scaffolds in the 3D shape. In this research will investigate and find a new polymer solution and the appropriate parameters that can be able to be fabricate the 3D polymer fibrous scaffold as similar as possible to the original shape. The 3D electrospinning methods are used to fabricate 3D scaffolds by using the modified 3D printing to printed the scaffolds from the positive electrode connected needle (printed into the negative electrode connected base) and syringe that contained the polymer solution and graphene oxide addition. The graphene oxide will be used as an additive because this carbon-based nanomaterial can enhance mechanical and biological properties of the 3D scaffolds. In this research used 5 different types of graphene as the additive and will be used the SEM, XRD, FTIR and Raman characterization to classify each type of graphene in the 3D polymer scaffolds. And this research also fabricated the 3D scaffolds without the additive for the comparison. Furthermore, polymer scaffolds fabricated by the 3D electrospinning techniques will be compared and characterized by using mechanical testing machine and the above characterizations.

Keywords: 3D electrospining; graphene; polycaprolactone

CURRICULUM VITAE

Name Tiprat Vitayakitpipat

Date of Birth February 28th 1998

Place of Birth Maharat Nakhon Ratchasima Hospital, Nakhon Ratchasima province

Education 2020- present
Master of Science in Physics Nakhon Ratchasima, Suranaree University of Technology, GPAX 3.80
2016- 2019
Bachelor of Science in Physics, Nakhon Ratchasima, Suranaree University of Technology, GPAX 3.60
2013- 2016
High School Diploma, Nakhon Raschasima, Suranaree Witthaya school, GPAX 3.79

Publications -

Awards -

Grants and Fellowships 2013- present
The development and promotion of science and technology talent project (DPST)

Position and Place of Work Master's degree student at Suranaree University of Technology